IEEE Access
Multidisciplinary | Rapid Review | Open Access Journal

Date of publication xxxx 00, 0000, date of current version xxxx 00, 0000.

Digital Object Identifier 10.1109/ACCESS.2017.Doi Number

Automatic Generation Control of a Future Multi-source Power System Considering High Renewables Penetration and Electric Vehicles: Egyptian Power System in 2035

Morsy Nour[1,2], Gaber Magdy[2], José Pablo Chaves-Ávila[1], Álvaro Sánchez-Miralles[1], Eduard Petlenkov[3]

[1]Institute for Research in Technology (IIT), ICAI School of Engineering, Comillas Pontifical University, 28015 Madrid, Spain
[2]Department of Electrical Engineering, Faculty of Energy Engineering, Aswan University, 81528 Aswan, Egypt
[3]Centre for Intelligent Systems, Department of Computer Systems, Tallinn University of Technology, 19086 Tallinn, Estonia

Corresponding author: Morsy Nour (mmohammed@comillas.edu), Gaber Magdy (gabermagdy@aswu.edu.eg)

The work of Eduard Petlenkov was supported by the Estonian Research Council under Grant PRG658

ABSTRACT Egypt aims to diversify electricity generation sources and targets 42% of its power capacity through different renewable energy sources (RESs) by 2035. Such an increased share of RESs will make grid operation and control more tedious and may have a negative impact on power system frequency stability. Therefore, this paper is the first study that studies the automatic generation control of future multi-source power systems (e.g., Egyptian Power System (EPS) in a future 2035 scenario) considering high RESs penetrations and electric vehicles (EVs). The RESs in this future scenario include photovoltaic plants, wind generation plants, concentrated solar power plants, and hydropower plants. The EPS also contains other traditional power plants based on fossil fuels (i.e., coal, oil, and natural gas) and nuclear power plants. Moreover, this study investigates the effect of participation of EVs in enhancing the frequency stability of the future-scenario EPS. Furthermore, this study proposes a fractional-order proportional integral derivative (FOPID) controller for load frequency control (LFC), and its parameters are tuned using RUNge Kutta optimizer (RUN), which is a new optimization algorithm. To assess the FOPID controller performance, it was compared with a proportional-integral-derivative controller, proportional-integral controller, and integral controller. The results showed the positive effect of EVs' participation in frequency regulation of the future-scenario EPS, the effectiveness of RUN optimizer in LFC application, and the superior performance of the FOPID controller over its peers of controllers used in the literature in improving frequency stability through reducing frequency deviations caused by different disturbances and under various power system conditions.

INDEX TERMS automatic generation control, Egyptian power system, electric vehicle, FOPID controller, frequency regulation, load frequency control, renewable energy sources.

NOMENCLATURE

Acronyms

EPS	Egyptian power system
ESS	Energy storage systems
EV	Electric vehicle
CSP	Concentrated solar power
PV	Photovoltaic
WG	Wind generation
RESs	Renewable energy sources
LFC	Load frequency control
FOPID	Fractional-order proportional integral derivative
I	Integral
P	Proportional
PI	Proportional integral
PID	Proportional integral derivative
GDB	Governor deadband
GRC	Generation rate constraint
RUN	RUNge Kutta optimizer
ABC	Artificial bee colony
PSO	Particle swarm optimization
IAE	Integral of absolute error
ISE	Integral of squared error
ITAE	Integral of time multiplied absolute error
ITSE	Integral of time multiplied squared error
IEA	International energy agency
IRENA	International renewable energy agency
ISES	Integrated sustainable energy strategy
MOS	Maximum overshoot
MUS	Maximum undershoot
Remap	Renewable energy roadmap

This article has been accepted for publication in a future issue of this journal, but has not been fully edited. Content may change prior to final publication. Citation information: DOI 10.1109/ACCESS.2022.3174080, IEEE Access

SLP	Step load perturbation
TS	Settling time (s)
P.F	Participation factor

Indices

Two-area power system parameters

Δf_1	Area 1 frequency deviation (Hz)
Δf_2	Area 2 frequency deviation (Hz)
ΔP_{tie}	Power deviation in tie-line between areas 1 and 2 (pu)
ΔP_C	Control signal to reheat thermal power plant (pu)
ΔP_M	Reheat thermal power plants power change (pu)
ΔP_L	Change in load power (pu)
$G_{ps}(s)$	Transfer function of power system
$G_g(s)$,	Transfer function of governor
$G_t(s)$,	Transfer function of turbine
$G_r(s)$	Transfer function of reheater
$G_{PID}(s)$	Transfer function of PID controller
$G_{PI}(s)$	Transfer function of PI controller
K_{ps}	Power system gain (Hz/pu MW)
K_r	Reheater gain
K_p	Proportional gain
K_i	Integral gain
K_d	Derivative gain
N	Derivative filter coefficient of the PID controller
T_{ps}	Power system time constant (s)
T_{tie}	Synchronization coefficient
T_g	The time constant of the governor (s)
T_t	The time constant of the turbine (s)
T_r	The time constant of the reheater (s)
R	Governor speed regulation (Hz/pu MW)
B	Bias constant (pu MW/Hz)
ACE	Area control error

Egyptian power system parameters

Δf	Egyptian power system frequency deviation (Hz)
ΔP_{m1}	Non-reheat thermal power plants power change (pu)
ΔP_{m2}	Reheat thermal power plants power change (pu)
ΔP_{m3}	Hydropower plants power change (pu)
ΔP_{m4}	Nuclear power plants power change (pu)
ΔP_{PV}	Photovoltaic plants power change (pu)
ΔP_{CSP}	Concentrated solar power plants power change (pu)
ΔP_{WG}	Wind generation plants power change (pu)
ΔP_{EVs}	Change of electric vehicles charging/discharging power (pu)
ΔP_L	Change in load power (pu)
ΔP_{C1}	Control signal to non-reheat thermal power plants
ΔP_{C2}	Control signal to reheat thermal power plants
ΔP_{C3}	Control signal to hydropower plants
ΔP_{C4}	Control signal to nuclear power plants
ΔP_{CEVs}	Control signal to aggregated EVs
ΔP_{Solar}	Power change of solar irradiance
ΔP_{CSP}	Power change of solar thermal
ΔP_{WG}	Power change of wind generation
H_{EPS}	EPS inertia constant (s)
D_{EPS}	EPS damping coefficient (pu MW/Hz)
K_{r2}	Reheater gain of reheat thermal power plants
K_H	High-pressure turbine gain of nuclear power plants
K_{R1}	Low-pressure turbine gain of nuclear power plants
K_{PV}	Photovoltaic generation gain
K_{SCSP}	Solar collector gain of CSP
K_{TCSP}	Turbine gain of CSP
K_{WG}	Wind generation gain
K_{av}	Average participation factor of EVs
λ	Fractional-order operator of FOPID controller
μ	Fractional-order operator of FOPID controller
N_{EV}	Total number of EVs
$P.F.1$	Participation factor of non-reheat thermal power plants
$P.F.2$	Participation factor of reheat thermal power plants
$P.F.3$	Participation factor of hydropower power plants
$P.F.4$	Participation factor of nuclear power plants
$P.F.5$	Participation factor EVs
R_1	Governor speed regulation of non-reheat thermal power plants (Hz/pu MW)
R_2	Governor speed regulation of reheat thermal power plants (Hz/pu MW)
R_3	Governor speed regulation of hydropower plants (Hz/pu MW)
R_4	Governor speed regulation of nuclear power plants (Hz/pu MW)
R_{av}	Average droop coefficient of EVs (Hz/pu MW)
T_{g1}	Governor time constant of non-reheat thermal power plants (s)
T_{t1}	Turbine time constant of non-reheat thermal power plants (s)
T_{g2}	Governor time constant of reheat thermal power plants (s)
T_{t2}	Turbine time constant of reheat thermal power plants (s)
T_{r2}	Reheat time constant of reheat thermal power plants (s)
T_3	Water gate time constant of hydro power plants (s)
T_d	Dashpot time constant of governor of hydropower plants (s)
T_w	Water starting time in hydro intake (s)
T_4	Governor time constant of nuclear power plants (s)
T_{T1}	High-pressure turbine time constant of nuclear power plants (s)
T_{RH1}	First low-pressure turbine time constant of nuclear power plants (s)
T_{RH2}	Second low-pressure turbine time constant of nuclear power plants (s)
T_{PV}	Time constant of photovoltaic generation (s)
T_{SCSP}	Solar collector time constant of CSP (s)
T_{TCSP}	Turbine time constant of CSP (s)
T_{WG}	Time constant of wind generation (s)
T_{EV}	Average time constant of EV chargers (s)
$G_{FOPID}(s)$	Transfer functions of FOPID controller

I. INTRODUCTION

There is a continuous and fast increase in electricity generation from renewable energy sources (RESs) worldwide. The RESs adoption is driven by environmental issues, the expectation of depletion of fossil fuels in the near future, an increase in energy needs due to the rise in population, and the need to increase energy security by diversifying the sources of energy and reducing the fuel imports from other countries. There are many technologies for electricity generation from renewable sources [1], [2]. However, electricity generation from wind and solar are the most widely used because these technologies are more mature and have lower costs than other renewable technologies such as geothermal, biomass, etc. [3].

This article has been accepted for publication in a future issue of this journal, but has not been fully edited. Content may change prior to final publication. Citation information: DOI 10.1109/ACCESS.2022.3174080, IEEE Access

A. LITERATURE REVIEW

The increasing share of RESs provides economic, environmental, and energy security advantages. However, it results in challenges in the operation and control of the power system and if not properly managed they may lead to blackouts [4] due to their intermittent and unpredictable nature as their power production depends on weather conditions. Additionally, they are generally non-dispatchable generation sources (i.e., cannot participate in frequency regulation in normal operation) and has no or low inertia because they are connected to the grid through power electronic converters [5], [6].

Considering these challenges associated with the high share of RESs on power system operation and control. The effect of the high share of RESs on power systems frequency stability gained considerable interest in research studies considering different RESs penetration levels, different RESs (i.e., photovoltaic (PV), wind generation (WG), etc.) [7], different case studies (interconnected power systems, isolated power systems, microgrids, etc.), and in the presence of various energy storage systems (ESSs).

Many studies found that ESSs will have a significant role in future power systems considering the reduction of the share of dispatchable generation (i.e., conventional generation). Many studies proved the technical feasibility of many ESSs in improving the frequency stability of power systems integrated by a high share of RESs [8]. For instance, the following studies proposed frequency stability improvement using batteries [9], [10], flywheels [11], superconducting magnetic energy storage (SMES) [12], pumped hydro energy storage [13], fuel cells [9], supercapacitors [14], etc. [15]. However, the high cost of these ESSs hinders their use on a wide scale till now. Therefore, researchers proposed using batteries of electric vehicles (EVs) when they are parked to provide grid services (i.e., frequency regulation, voltage regulation, improving power quality, load leveling, etc.). This interest in using EVs as energy storage to provide grid services is driven by the continuous and fast increase of EVs number worldwide. The international energy agency (IEA) 2020 EVs outlook report showed that EVs stock exceeded 7 million in 2019. Based IEA report, it is expected that EVs number will be between 140 and 245 million in 2030 [16].

Many controllers were proposed in the literature for the load frequency control (LFC) of power systems. Furthermore, numerous control strategies have been applied for the frequency stability of power systems including model predictive control [17], reinforcement learning [18], sliding mode control [19], fuzzy logic control [20], fuzzy-PID [21], artificial neural network [22], coefficient diagram method [23], etc. On the other hand, researchers have turned their efforts towards the use of the proportional integral derivative (PID) controller and its modifications due to their simplicity in configuration, inexpensiveness, and a wide margin of stability [24]. Despite this, when dealing with system nonlinearities, these controllers have difficulty in determining their parameters via trial and error approaches. Considering the experience and effort needed to tune the frequency controller, the controller parameters are usually tuned using optimization techniques, mostly nature-inspired optimization algorithms in recent years due to their effectiveness in real-world applications [25]–[27].

The integration of EVs into power systems and how they can be used to provide grid services in general and frequency regulation particularly received significant interest from researchers [28], [29]. For instance, reference [30] proved the feasibility of EVs and battery energy storage in improving the frequency stability of a two-area power system, fastening response rate, enabling the integration of a higher share of RESs, and reducing the reserve capacity requirement. Another study [31] proposed a fractional-order proportional integral derivative (FOPID) controller for frequency regulation in a multi-area deregulated power system containing conventional generation. The results showed that EVs operating in V2G mode enhanced frequency stability by compensating uncontracted extra load demand. The authors of [32] used EVs to improve the frequency stability of a microgrid containing diesel generators, PV, and wind generations. They used an integral controller to control microgrid frequency, and the controller gain was tuned using the Harris hawks optimization (HHO) algorithm. In [33], the results proved the effectiveness of EVs in improving the frequency stability of three-area interconnected microgrids. The microgrids contain diesel generators, PV, WG, solar thermal generation, and biogas generation.

B. RESEARCH GAP AND MOTIVATION

Based on Egypt's integrated sustainable energy strategy to 2035 (ISES 2035) [34], Egypt aims to diversify the sources for electricity generation to reduce fuel imports and increase energy security and targets to increase the share of RESs to reach 42% of the generation capacity in 2035. The installed RESs will include PV, WG, concentrated solar power (CSP), and hydropower plants. Moreover, RESs generation will be complemented by nuclear power plants and other conventional power plants based on fossil fuels (i.e., coal, oil, and natural gas). This increase in RESs share will make grid operation and control more tedious and may have a negative impact on power system frequency stability. Therefore, there is a need for studies to assess the frequency stability of the EPS in this future scenario.

Egypt has no announced targets for EVs deployment in the long term. However, in the recent report published by the International Renewable Energy Agency (IRENA) and the Egypt Ministry of Electricity and Renewable Energy, it is estimated that the EVs number in Egypt could reach 700,000 in 2030 based on IRENA renewable energy roadmap (REmap) [34]. Based on these expectations of high RESs integration and high EVs deployment in Egypt in the future, this paper assesses the frequency stability of the EPS and investigates

This article has been accepted for publication in a future issue of this journal, but has not been fully edited. Content may change prior to final publication. Citation information: DOI 10.1109/ACCESS.2022.3174080, IEEE Access

how EVs can enhance the frequency stability of future EPS in 2035 if they are allowed to provide frequency regulation.

C. CONTRIBUTION AND PAPER ORGANIZATION

The main contributions of this paper are summarized in the following points:

- To the best of our knowledge, this is the first study to assess the frequency stability of multi-source Egyptian power system in the 2035 future scenario considering high RESs penetrations and EVs. In this scenario, RESs represent 42% of the generation capacity.
- Enhancing the frequency stability of the EPS using EVs. Where the EVs support the conventional generation to balance supply and demand considering the continuous loads and RESs generation variations.
- A new optimization algorithm called RUN is proposed for the LFC application. It was compared with well-known optimization algorithms such as particle swarm optimization (PSO) and artificial bee colony (ABC) algorithms in a two-area interconnected power system. The RUN algorithm showed a better performance in tuning the parameters of frequency controllers for the LFC of the test system compared to the other optimization algorithms.
- The FOPID controller is proposed for the LFC of a real future power system (i.e. EPS) with a high share of RESs. Also, to get the best performance from the proposed controller, its parameters are tuned using RUN.
- The RUN-based FOPID controller performance is compared with PID, PI, and I controllers. The results proved the proposed controller's better performance in improving frequency stability and reducing frequency deviations resulting from different disturbances and under various operating conditions of EPS and large changes in EPS inertia constant (H).

This paper is organized as follows. Section II presents a two-area interconnected power system to test the effectiveness of the proposed optimization algorithm for LFC application. Section III presents the structure and the dynamic model of the EPS in the 2035 scenario and aggregated model of EVs. Section IV presents the proposed FOPID controller, problem formulation, and objective function. Results and discussions are provided in section V. Finally, the study conclusion is presented in section VI.

II. TWO-AREA INTERCONNECTED POWER SYSTEM

To test the performance of the proposed optimization, a widely used test system is used. The test system is a two-area interconnected power system. The two areas are identical, and each area contains thermal generation with reheat, as shown in Fig. 1, which shows the block diagram representation of the power system dynamic model. The transfer functions of power system $G_{ps}(s)$, governor $G_g(s)$, turbine $G_t(s)$, and reheater $G_r(s)$ are given in equations (1) to (4) respectively. Where k_{ps} is power system gain, and k_r is reheater gain. T_{ps} is the power system time constant, T_g is governor time constant, T_t is turbine time constant, and T_r is reheater time constant. R is speed regulation, B is area frequency bias parameter, and T_{tie} is synchronization coefficient. The system power base is 2000 MVA, the area rated power capacity is 2000 MVA, and the rated load demand is 1000 MW. The power system parameters are given in Appendix 1 [35].

$$G_{ps}(\mathrm{s}) = \frac{K_{ps}}{T_{ps}s + 1} \tag{1}$$

$$G_g(\mathrm{s}) = \frac{1}{T_g s + 1} \tag{2}$$

$$G_t(\mathrm{s}) = \frac{1}{T_t s + 1} \tag{3}$$

$$G_r(\mathrm{s}) = \frac{K_r T_r s + 1}{T_r s + 1} \tag{4}$$

A. LFC USING PID CONTROLLER

Till now PID controller is the most used controller in the industry because of its simplicity and good performance. Depending on the application, one loop or more (i.e. proportional (P), I, PI, etc.) can be used to achieve the best performance. Therefore, PID controller (e.g., I controller and PI controller) is still widely used for LFC at power systems control centers. In this study, the proposed optimization algorithm is used to tune the parameters of a PID controller with a filter at the derivative branch. The PID controller transfer function in the s-domain is given in (5), and its block diagram representation is shown in Fig. 2. Furthermore, the PI controller transfer function in the s-domain is given in (6), and its block diagram representation is shown in Fig. 3.

$$G_{PID}(s) = K_p + \frac{K_i}{s} + K_d \frac{N}{1 + N\frac{1}{s}} \tag{5}$$

$$G_{PI}(s) = K_p + \frac{K_i}{s} \tag{6}$$

where $G_{PID}(s)$ is PID controller transfer function and $G_{PI}(s)$ is PI controller transfer function. K_p is the proportional gain, K_i is the integral gain, K_d is the derivative gain, and N is the derivative filter coefficient. The PID controller is proposed for the two-area power system, and the four design variables (i.e., K_p, K_i, K_d, and N) are the parameters that the proposed optimization algorithm is used to tune. The PID controller parameters are subjected to limits as given in (7) to (10). The same limits apply to controllers at area 1 and area 2.

This article has been accepted for publication in a future issue of this journal, but has not been fully edited. Content may change prior to final publication. Citation information: DOI 10.1109/ACCESS.2022.3174080, IEEE Access

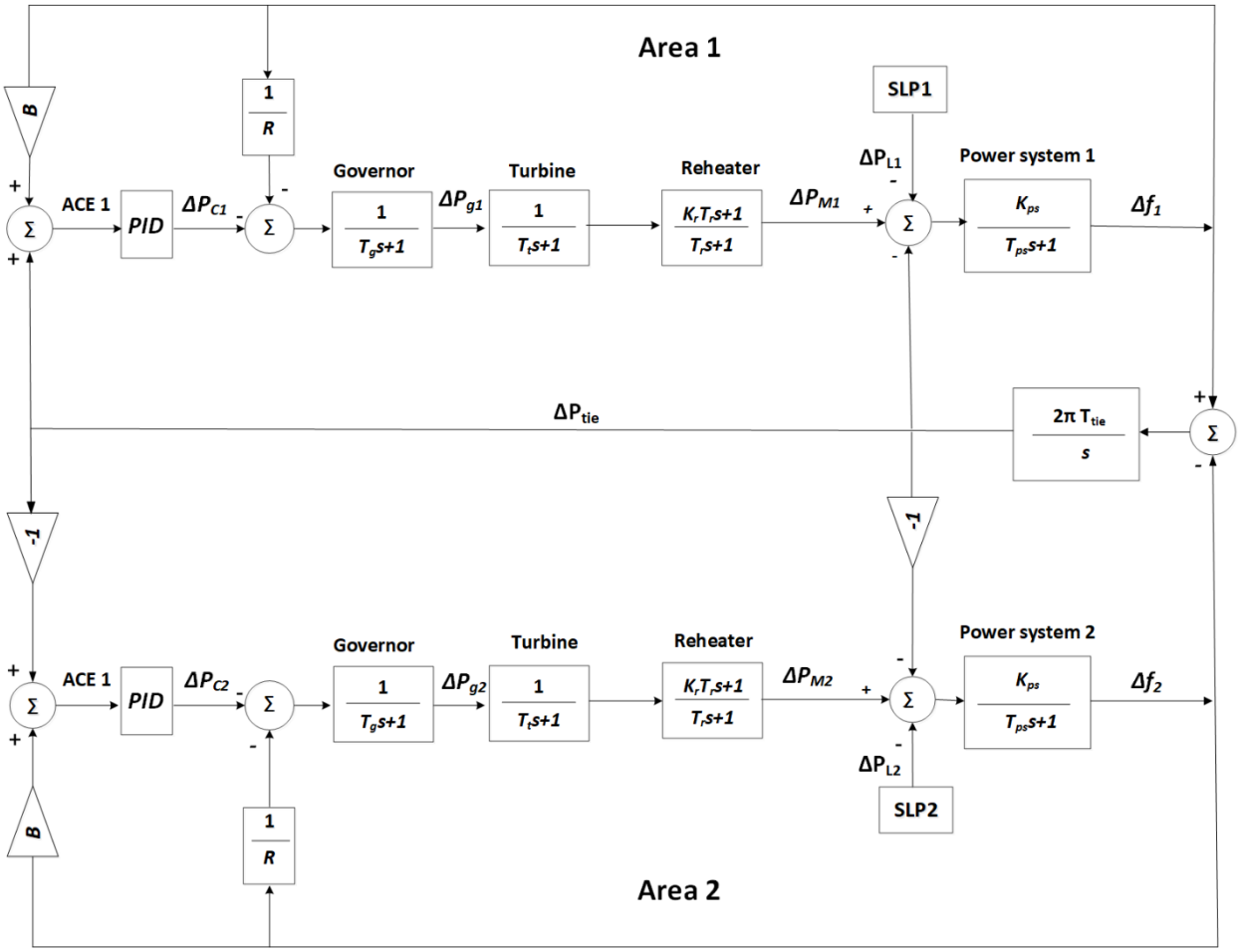

FIGURE 1. Block diagram of the tested two-area power system.

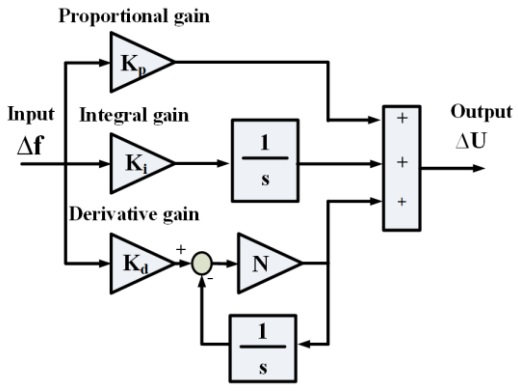

FIGURE 2. Structure of the PID controller.

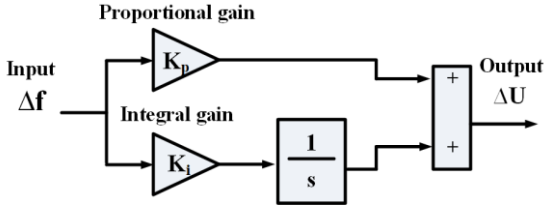

FIGURE 3. Structure of the PI controller.

$$K_p^{min} \le K_{p1}, K_{p2} \le K_p^{\max} \quad (7)$$

$$K_i^{min} \le K_{i1}, K_{i2} \le K_i^{\max} \quad (8)$$

$$K_d^{min} \le K_{d1}, K_{d2} \le K_d^{\max} \quad (9)$$

$$N^{min} \le \mathrm{N}_1, \mathrm{N}_2 \le N^{max} \quad (10)$$

B. RUNGE KUTTA (RUN) OPTIMIZER

The RUN algorithm is an optimization algorithm that is recently developed by [36]. The RUN is a population-based algorithm, and its design is based on the foundations of the Runge Kutta mathematical method that is widely used to solve ordinary differential equations. The RUN consists of two parts, Runge Kutta method-based search mechanism and a mechanism to enhance the solution quality. Fig. 4 shows a flowchart of the RUN algorithm. In this subsection, a brief description of the algorithm and main equations are presented, and a detailed explanation of RUN can be found in [36].

This article has been accepted for publication in a future issue of this journal, but has not been fully edited. Content may change prior to final publication. Citation information: DOI 10.1109/ACCESS.2022.3174080, IEEE Access

1. Initialization

In the first step, random initial positions of decision variables are generated by (11)

$$X_{n,l} = L_l + rand.(U_l - L_l) \quad (11)$$

where x_n is one of the solutions (n = 1, 2, …, N). N is the population size, l refers to a variable in the solution, (l = 1, 2, …, D). D is the optimization problem dimension. L_l is the lower bound of l_{th} variable, U_l is the upper bound of l_{th} variable, *rand* is a random number in the range from 0 to 1.

2. Root of search mechanism

In the RUN algorithm, RK4 is used to determine the search mechanism. In this step four weighing factors k_1, k_2, k_3, and k_4 are calculated.

3. Updating solutions

The RUN algorithm uses the Runge Kutta method to update the positions of the solution at each iteration. The equation to update the positions is given in (12).

$if\ rand < 0.5$

(exploration phase)

$$x_{n+1} = (x_c + r \times SF \times g \times x_c) + SF \times SM + \mu \times x_s$$

else

(Exploitation phase)

$$x_{n+1} = (x_m + r \times SF \times g \times x_m) + SF \times SM + \mu \times x_s,$$

end (12)

4. Enhancing solution quality

This step aims to escape from local optima, improve the obtained solutions, and ensure fast convergence. To achieve this, three new solutions (x_{new1}, x_{new2}, and x_{new3}) are calculated using the following equations:

if rand < 0.5

if w < 1

$$x_{new2} = x_{new1} + r.w.\left|(x_{new1} - x_{avg}) + randn\right|$$

else

$$x_{new2} = (x_{new1} - x_{avg}) + r.w.\left|(u.x_{new1} - x_{avg}) + randn\right|$$

end

end (13)

in which

$$w = rand(0,2).\exp\left(-c\left(\frac{i}{Maxi}\right)\right) \quad (13\text{-}1)$$

$$x_{avg} = \frac{x_{r1}+x_{r2}+x_{r3}}{3} \quad (13\text{-}2)$$

$$x_{new1} = \beta \times x_{avg} + (1-\beta) \times x_{best} \quad (13\text{-}3)$$

if rand < w

$$x_{new3} = (x_{new2} - rand.x_{new2}) + SF.(rand.x_{RK} + (v.x_b - x_{new2})) \quad (14)$$

end

The values or equations to calculate all the unknowns (i.e., *SF*, *SM*, *r*, etc.) mentioned in the previous equations can be found in [36]. In [36], the RUN algorithm was compared with many recent optimization algorithms and it showed many merits compared to them such as good exploration and exploitation abilities, effectiveness in many real-world optimization problems, requiring the setting of only two control parameters, and has low sensitivity to change of control parameters values. Furthermore, few studies showed the good performance of this new optimization algorithm in optimizing different engineering optimization problems. Therefore, in this study, the RUN algorithm is used to design a robust controller for LFC application.

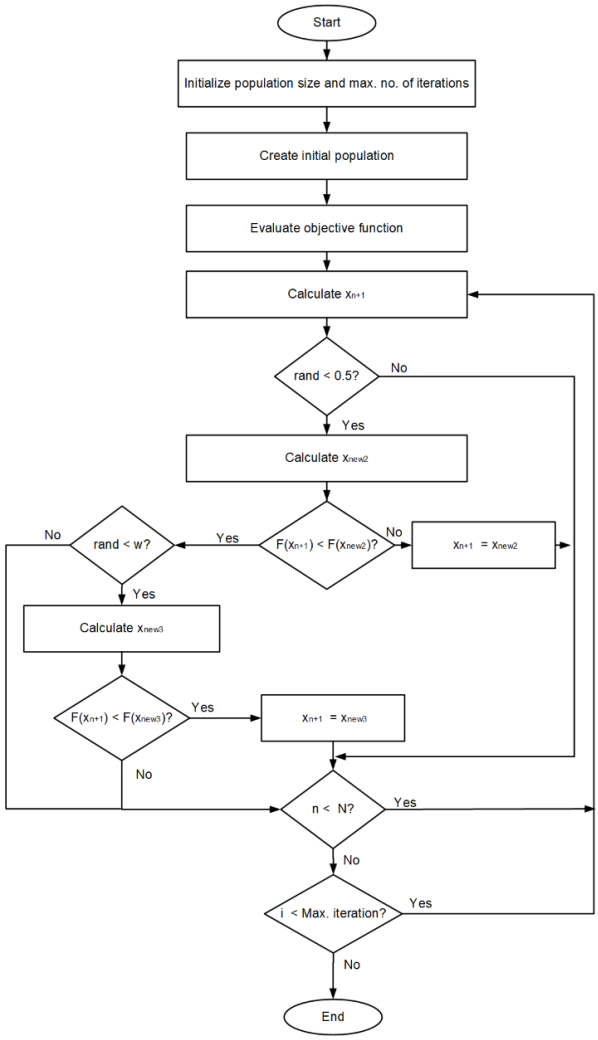

FIGURE 4. Flow chart of the RUN optimization algorithm.

C. SELECTION OF OBJECTIVE FUNCTION

Many performance indices were used as objective functions to tune controllers' parameters in the literature. In this subsection, the performance of four widely used objective functions is compared to select one objective function that provides the best performance for the two-area power system under study. The considered objective

This article has been accepted for publication in a future issue of this journal, but has not been fully edited. Content may change prior to final publication. Citation information: DOI 10.1109/ACCESS.2022.3174080, IEEE Access

functions are integral of time multiplied absolute error (*ITAE*), integral of absolute error (*IAE*), integral of time multiplied squared error (*ITSE*), integral of squared error (*ISE*), and their equations are given in equations (15) to (18), respectively. The objective of the proposed optimization algorithm (i.e., RUN algorithm) is to fine-tune the parameters of the frequency controller that will result in the lowest value of these objective functions. Low values of objective functions correspond to good frequency response with low-frequency deviations and settling time after the occurrence of a disturbance.

$$ITAE = \int_0^{tsim} (|\Delta f_1| + |\Delta f_2| + |\Delta P_{tie}|) * t\, dt \quad (15)$$

$$IAE = \int_0^{tsim} (|\Delta f_1| + |\Delta f_2| + |\Delta P_{tie}|)\, dt \quad (16)$$

$$ITSE = \int_0^{tsim} (\Delta f_1^2 + \Delta f_2^2 + \Delta P_{tie}^2) * t\, dt \quad (17)$$

$$ISE = \int_0^{tsim} (\Delta f_1^2 + \Delta f_2^2 + \Delta P_{tie}^2)\, dt \quad (18)$$

Where Δf_1 is frequency deviation at area 1, Δf_2 is frequency deviation at area 2, ΔP_{tie} is power deviation in the tie-line between area 1 and area 2, and t_{sim} is simulation time. The PID controller is tuned using each objective function individually based on the proposed RUN algorithm, and the optimal controller parameters for the four objective functions are given in Table 1.

The controllers' parameters are turned using the RUN algorithm under the following conditions. +0.01pu step load perturbation (SLP)`in area 1 at time t = 0 s, the PID controller limits from 0 to 10 for gains (i.e., k_p, k_i, and k_d) and 0 to 100 for filter coefficient (i.e. N). The optimization algorithm parameters are 20 population size and 100 iterations. The best value of the objective function obtained in 5 runs is selected.

The comparison between the four objective functions is given in Fig. 5, which shows Δf_1, Δf_2, and ΔP_{tie}. Furthermore, the maximum undershot (MUS), maximum overshoot (MOS), and setting time (T_S) based on ± 0.005% criterion for Δf_1, Δf_2, and ΔP_{tie} are given in Table 2. From the simulation results presented in Fig. 5 and Table 2, it can be noticed that the ISE objective function provides the lowest value of MUS compared to other objective functions for Δf_1, Δf_2, and ΔP_{tie}, and provides lower T_S for Δf_1 and Δf_2. Considering that MUS is very significant in the frequency stability analysis of power systems, the PID controller parameters based on the RUN algorithm which is tuned using the objective "ISE" will be used for comparison with other optimization algorithms.

D. RESULTS AND DISCUSSION

The proposed RUN optimization algorithm is used to tune the PID controller parameters, and the controller parameters are given in Table 1 for the selected ISE objective function. The RUN based PID controller (i.e., RUN-PID) performance is compared with ABC based PID (i.e., ABC-PID) and PI controllers (i.e., ABC-PI) [35] in addition to PSO based PI controller (i.e., PSO-PI) [37] under various disturbances and operating conditions as described in the following scenarios.

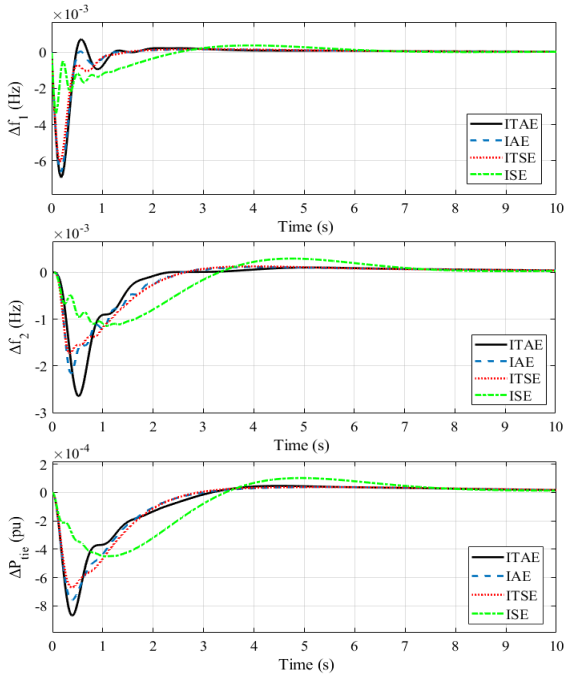

FIGURE 5. System response for different objective functions. (a) Δf_1, (b) Δf_2, and (c) ΔP_{tie}.

Scenario 1: System performance assessment under 1% sudden load change in area 1

In this scenario, a + 0.01 pu SLP is applied in area 1, and Δf_1, Δf_2, and ΔP_{tie} are recorded. The performance of the proposed RUN-PID controller is compared with ABC-PID, ABC-PI, and PSO-PI controllers. The dynamic response of Δf_1, Δf_2, and ΔP_{tie} are given in Fig. 6, and their corresponding MUS, MOS, and Ts are given in Table 3. The results show that the proposed RUN-PID controller provides better performance compared to other controllers. Where the proposed RUN-PID controller showed smaller deviations and faster settling times (i.e. better values in all performance indices) than ABC-PID, ABC-PI, and PSO-PI controllers. This proves the effectiveness and superiority of the proposed optimization algorithm in LFC application compared to other optimization algorithms (e.g., PSO and ABC).

Scenario 2: System performance assessment under 5% sudden load change in area 1

In this scenario, the robustness of the proposed RUN-PID controller is tested by applying a 0.05 pu SLP in area 1. The parameters of the designed PID controller based on the RUN optimization algorithm used in this scenario are given in Table 1. Δf_1, Δf_2, and ΔP_{tie} for this scenario are displayed in

This article has been accepted for publication in a future issue of this journal, but has not been fully edited. Content may change prior to final publication. Citation information: DOI 10.1109/ACCESS.2022.3174080, IEEE Access

Fig. 7, and corresponding MUS, MOS, and Ts are given in Table 3. The results showed the robustness of the proposed RUN-PID controller and its efficient performance under different magnitudes of SLPs.

Table 1. Optimal values of PID controller parameters for different objective functions

Objective functions		Area 1				Area 2			
		K_p	K_i	K_d	N	K_p	K_i	K_d	N
ITAE	0.016149	10	10	2.0785	99.9138	3.6732	10	2.2649	55.0300
IAE	0.0067013	10	10	2.3348	100	10	10	8.2322	33.2799
ITSE	4.3994E-6	10	10	2.8672	100	10	10	10	60.7844
ISE	6.272E-6	10	10	10	100	10	10	10	100

Table 2. Performance indices values for different objective functions

Objective functions	Δf_1			Δf_2			ΔP_{tie}		
	MUS (Hz)	MOS (Hz)	T_S (s)	MUS (Hz)	MOS (Hz)	T_S (s)	MUS (pu)	MOS (pu)	T_S (s)
ITAE	6.926E-3	7.166E-4	8.00	2.640E-3	1.019E-4	9.00	8.690E-4	4.712E-5	2.35
IAE	6.614E-3	1.586E-4	7.80	2.161E-3	1.143E-4	8.95	7.607E-4	3.916E-5	2.36
ITSE	6.040E-3	1.712E-4	7.64	1.739E-3	1.267E-4	8.82	6.707E-4	3.907E-5	2.36
ISE	3.380E-3	3.773E-4	6.84	1.147E-3	2.932E-4	7.70	4.506E-4	1.027E-4	6.91

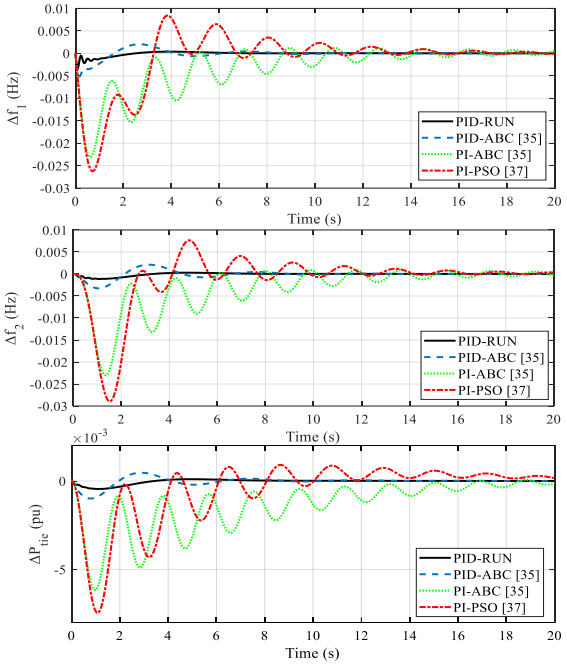

FIGURE 6. System response for scenario 1. (a) Δf_1, (b) Δf_2, and (c) ΔP_{tie}.

Scenario 3: System performance assessment under system uncertainties

In this scenario, a sensitivity analysis is performed to test the robustness of the proposed optimized controller to changes in system parameters from its nominal values. The parameters (i.e., k_{ps}, T_{ps}, and T_{tie}) are changed by ± 25% from the nominal values. Moreover, a 0.01 pu SLP is applied in area 1. The results of all studied parameter variations are presented in Table 4, which shows MUS, MOS, and T s for Δf_1, Δf_2, and ΔP_{tie}. There was a negligible effect of the parameter change on power system dynamic response. Therefore, the results prove the effectiveness and robustness of the proposed RUN-PID for different changes in system parameters. All the studied scenarios show the excellent performance of the PID controller optimized using the proposed RUN algorithm. The excellent performance of the controller proves the viability of the proposed RUN algorithm in the LFC application. Consequently, in the following sections, the RUN algorithm will be used to optimize the parameters of different controllers (i.e., FOPID, PID, PI, and I controllers) considering EPS in the 2035 future scenario as a case study.

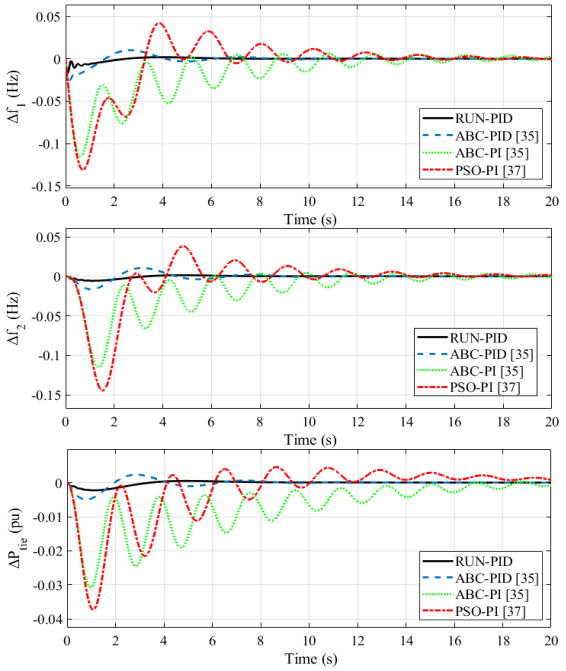

FIGURE 7. System response for scenario 2. (a) Δf_1, (b) Δf_2, and (c) ΔP_{tie}.

III. DYNAMIC MODEL OF THE EGYPTIAN POWER SYSTEM

For the last decades, the EPS contained conventional generation such as hydropower plants and thermal power plants powered by oil and natural gas with a minimal share of RESs such as Gabel El-Zeit and Zafarana wind farms. However, the Ministry of Electricity and Renewable Energy announced in 2015 the ISES 2035 [34]. In this strategy, Egypt aims to diversify the sources for electricity generation to reduce fuel imports and increase energy security and

This article has been accepted for publication in a future issue of this journal, but has not been fully edited. Content may change prior to final publication. Citation information: DOI 10.1109/ACCESS.2022.3174080, IEEE Access

targets to increase the share of RESs to reach 42% of the generation power capacity in 2035. The installed RESs will include PV, WG, CSP plants, and hydropower plants. Moreover, the EPS will contain nuclear power plants besides other conventional power plants that operate with fossil fuels.

Table 3. Performance indices values for scenario 1 and 2

	Optimal Controller	Δf_1			Δf_2			ΔP_{tie}		
		MUS (Hz)	MOS (Hz)	T_S (s)	MUS (Hz)	MOS (Hz)	T_S (s)	MUS (pu)	MOS (pu)	T_S (s)
Scenario 1	RUN-PID	3.380E-3	3.773E-4	6.84	1.147E-3	2.932E-4	7.70	4.506E-4	1.027E-4	6.91
	ABC-PID	5.162E-3	2.021E-3	12.36	3.261E-3	2.108E-3	12.94	9.932E-4	4.681E-4	8.38
	ABC-PI	2.308E-2	1.221E-3	37.31	2.303E-2	9.157E-4	40.00	6.169E-3	1.620E-4	43.72
	PSO-PI	2.623E-2	8.447E-3	27.65	2.896E-2	7.664E-3	28.78	7.462E-3	9.148E-4	26.00
Scenario 2	RUN-PID	1.686E-2	1.884E-3	15.62	5.736E-3	1.466E-3	16.17	2.253E-3	5.134E-4	13.05
	ABC-PID	2.584E-2	1.013E-2	16.94	1.633E-2	1.056E-2	17.59	4.978E-3	2.349E-3	16.70
	ABC-PI	1.154E-1	6.235E-3	48.52	1.151E-1	4.697E-3	53.15	3.084E-2	8.133E-4	54.80
	PSO-PI	1.312E-1	4.225E-2	36.35	1.448E-1	3.840E-2	35.29	3.731E-2	4.601E-3	28.43

Table 4. Performance indices values for scenario 3

System parameters	Change (%)	Δf_1			Δf_2			ΔP_{tie}		
		MUS (Hz)	MOS (Hz)	T_S (s)	MUS (Hz)	MOS (Hz)	T_S (s)	MUS (pu)	MOS (pu)	T_S (s)
k_{ps}	+25%	3.747E-3	3.742E-4	6.85	1.179E-3	2.861E-4	7.70	4.514E-4	1.022E-4	6.91
	-25%	2.689E-3	3.808E-4	6.89	1.133E-3	3.031E-4	7.65	4.540E-4	1.037E-4	6.87
T_{ps}	+25%	2.964E-3	3.803E-4	6.87	1.136E-3	3.008E-4	7.65	4.537E-4	1.034E-4	6.88
	-25%	3.837E-3	3.731E-4	6.85	1.193E-3	2.842E-4	7.72	4.521E-4	1.021E-4	6.91
T_{tie}	+25%	3.364E-3	3.553E-4	6.94	1.199E-3	2.994E-4	7.58	4.671E-4	1.052E-4	6.85
	-25%	3.394E-3	4.222E-4	6.74	1.068E-3	2.784E-4	7.83	4.283E-4	9.791E-5	6.98

The evolution of the installed generation capacity and sources between 2010 to 2035 is presented in Table 5, and they are displayed graphically in Fig. 8. This rapid increase of the EPS capacity and change of electricity generation mix to include a high share of RESs can make grid operation and control more tedious and complex. Consequently, various studies for future EPS operation and control are essential. This study focuses on assessing the frequency stability of future EPS in 2035 and dynamic response enhancement by controlling the charging and discharging of a large number of EVs to participate in frequency regulation.

A simplified schematic representation of the EPS generation mix is shown in Fig. 9. In addition, it shows the presence of loads and aggregated EVs. As shown in Fig. 9, future EPS contains conventional power plants and RESs. Conventional power plants include non-reheat thermal power plants, reheat thermal power plants, and nuclear power plants. In the EPS, thermal power plants use different fossil fuels for operation such as natural gas, oil, and coal. The RESs generation includes PV, CSP, WG, and hydropower plants (hydropower plants can also be considered conventional power plants).

The total generation capacity of the EPS in 2035 will be 146.7 GW distributed as follows: 39.65 GW for non-reheat thermal power plants, 39.65 GW for reheat thermal power plants (note that the capacity of fossil fuel-powered thermal power plants is divided equally between non-reheat and reheat thermal power plants since there is no information available about it at 2035 scenario), 4.8 GW for nuclear power plant, 2.9 GW for hydropower plants, 31 GW for PV, 8.1 GW for CSP plants, and 20.6 GW for WG. The dynamic model of the EPS based on the 2035 scenario considering EVs aggregated model is shown in Fig. 10. Transfer functions representation is used to model different components of EPS. To get accurate results, non-linearities such as governor deadband (GDB) and generation rate constraint (GRC)) are considered. Aggregated EVs and all controllable generation are responsible for keeping frequency within nominal limits and they receive their control signals from a centralized controller. Loads and intermittent RESs (i.e., ΔP_L, ΔP_{PV}, ΔP_{CSP}, and ΔP_{WG}) are the sources of fluctuations and disturbances in the grid under study since they are uncontrollable and difficult to forecast. All parameters of the EPS dynamic model are given in Appendix 2. The dynamic model of conventional power plants, RES, and aggregated EVs are explained in the following subsections.

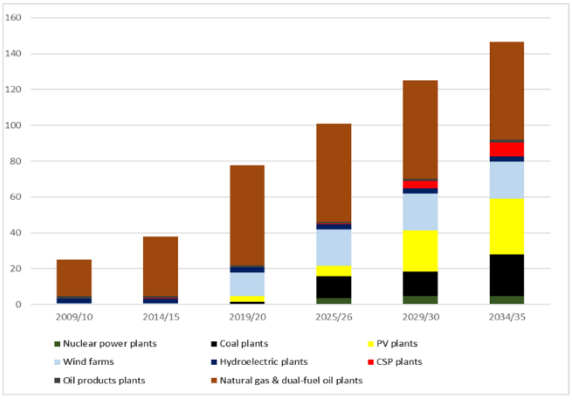

FIGURE 8. Evolution of installed generation capacity in Egypt from 2010 to 2035 in GW.

This article has been accepted for publication in a future issue of this journal, but has not been fully edited. Content may change prior to final publication. Citation information: DOI 10.1109/ACCESS.2022.3174080, IEEE Access

Table 5. Evolution of installed generation capacity in Egypt from 2010 to 2035 in GW

Power Plants	2009/10	2014/15	2019/20	2025/26	2029/30	2034/35
Nuclear power plants	0	0	0	3.6	4.8	4.8
Coal plants	0	0	1.6	12	13.6	23.2
PV plants	0	0	3	5.9	22.9	31
Wind farms	0.5	0.5	13.3	20.5	20.6	20.6
Hydroelectric plants	2.8	2.8	2.8	2.9	2.9	2.9
CSP plants	0	0.1	0.1	0.1	4.1	8.1
Oil products plants	1.4	1.3	0.9	1	1.3	1.3
Natural gas & dual-fuel oil plants	20.4	33	55.9	54.9	55	54.8
Total	**25.1**	**37.7**	**77.6**	**100.9**	**125.2**	**146.7**

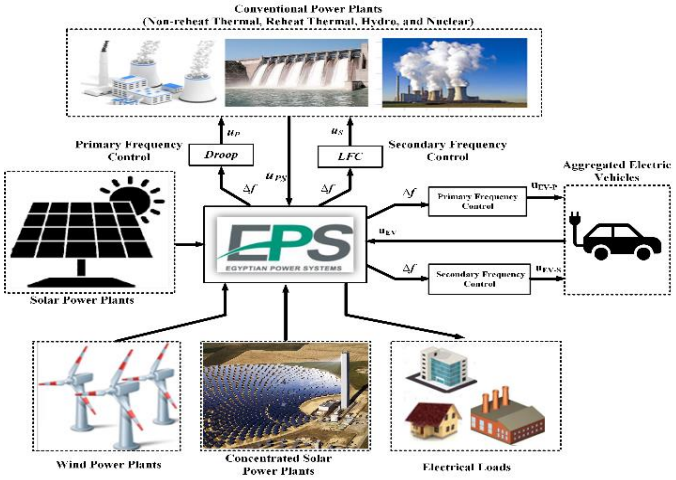

FIGURE 9. Schematic diagram of the EPS.

A. DYNAMIC MODEL OF CONVENTIONAL POWER PLANTS

Even in the 2035 future scenario, conventional generation (i.e., thermal and nuclear power plants) still represents a higher share of generation capacity than RESs. In this study, the GRC is defined as 20%/min for non-reheat power plants and reheat power plants, and 50%/min for hydropower plants. The GDB is defined as 0.06% for non-reheat power plants, 0.06% for reheat power plants, and 0.01% for hydropower plants. The power change of conventional power plants of the EPS is given in the following equations.

- **Non-reheat thermal power plants**

The non-reheat thermal power plants dynamic model is represented as in (19), which is given by [35], [38].

$$\Delta P_{m1} = \frac{1}{T_{g1}s+1} * \frac{1}{T_{t1}s+1}\left(\frac{-1}{R_1} * \Delta f - \Delta P_{c1}\right) \quad (19)$$

where ΔP_{m1}, T_{g1}, T_{t1}, R_1, and ΔP_{c1} represent non-reheat thermal power plants power change, governor time constant, turbine time constant, governor speed regulation, and control signal from the secondary controller to non-reheat thermal power plants, respectively. Moreover, Δf is frequency deviation and s is a complex number ($s = \sigma + j\omega$).

- **Reheat thermal power plants**

The reheat thermal power plants dynamic model is represented as in (20), which is given by [35], [38].

$$\Delta P_{m2} = \frac{1}{T_{g2}s+1} * \frac{1}{T_{t2}s+1} * \frac{K_{r2}T_{r2}s+1}{T_{r2}s+1} * \left(\frac{-1}{R_2} * \Delta f - \Delta P_{c2}\right) \quad (20)$$

where ΔP_{m2}, T_{g2}, T_{t2}, T_{r2}, k_{r2}, R_2, and ΔP_{c2} represent reheat thermal power plants power change, governor time constant, turbine time constant, reheater time constant, reheater gain, governor speed regulation, and control signal from the secondary controller to reheat thermal power plants, respectively.

- **Hydropower plants**

The hydropower plants dynamic model is represented as in (21), which is given by [38].

$$\Delta P_{m3} = \frac{T_d s+1}{T_3 s+1} * \left(\frac{-T_w s+1}{0.5 * T_w s+1}\right) * \left(\frac{-1}{R_3} * \Delta f - \Delta P_{c3}\right) \quad (21)$$

where ΔP_{m3}, R_3, and ΔP_{c3} represent hydropower plants power change, governor speed regulation, and control signal

This article has been accepted for publication in a future issue of this journal, but has not been fully edited. Content may change prior to final publication. Citation information: DOI 10.1109/ACCESS.2022.3174080, IEEE Access

from the secondary controller to hydropower plants, respectively. In addition, T_3, T_d, and T_w are hydropower plant water gate time constant, dashpot time constant of speed governor, and water starting time in hydro intake, respectively.

- **Nuclear power plants**

Egypt is constructing nuclear power plants and aims to reach a 4.8 GW generation capacity in 2035. The nuclear power plants dynamic model is represented as in (22), which is given by [39]. The model consists of a speed governor, a high-pressure turbine, and two low-pressure turbines.

$$\Delta P_{\mathrm{m4}} = \frac{1}{T_4 s+1} * \left(\frac{K_{\mathrm{H}}}{T_{\mathrm{T1}} s+1} + \frac{K_{\mathrm{R1}}}{(T_{\mathrm{T1}} s+1)(T_{\mathrm{RH1}} s+1)} + \frac{1-K_{\mathrm{H}}-K_{\mathrm{R1}}}{(T_{\mathrm{T1}} s+1)(T_{\mathrm{RH2}} s+1)} \right) * \left(\frac{-1}{R_4} * \Delta f - \Delta P_{c4} \right) \quad (22)$$

where ΔP_{m2}, K_H, K_{R1}, R_1, and ΔP_{c4} represent nuclear power plants power change, high-pressure (HP) turbine gain, first low-pressure (LP) turbine gain, governor speed regulation, and control signal from the secondary controller to nuclear power plants, respectively. Moreover, T_4, T_{T1}, T_{RH1}, and T_{RH2} represent nuclear power plants speed governor time constant, HP turbine time constant, first LP turbine time constant, and second LP turbine time constant, respectively.

B. DYNAMIC MODEL OF INTERMITTENT RENEWABLE ENERGY SOURCES

- **PV power plants**

PV is one of the most promising RESs worldwide besides WG. It is expected to be the main RES in Egypt because of the high solar irradiation all year and large free areas of the desert that can be used for PV power stations installations. Currently, Egypt produces 1465 MW from PV and targets to generate 31 GW in 2035. In this study, the PV generation dynamic model is represented as in (23), which is given by [40].

$$\Delta P_{PV} = \left(\frac{K_{PV}}{T_{PV} s+1} \right) * \Delta P_{\mathrm{Solar}}. \quad (23)$$

where K_{PV} and T_{PV} are PV generation gain and time constant. ΔP_{Solar} represents power change of solar irradiance and ΔP_{PV} represents power change of PV generation.

PV power output is variable and difficult to predict because it depends on weather conditions (i.e., solar irradiation). Therefore, it is a non-dispatchable generation and represents a source of fluctuation and disturbance in the power system under study. Additionally, it has no inertia because it is connected to the grid through a power electronic-based converter. Consequently, it reduces the power system inertia.

- **CSP plants**

The energy from the sun can be captured in the form of light in PV generation or the form of heat as in the thermal CSP plants. CSP plants are suitable in Egypt because of the high solar irradiation, hot weather, and large free areas of desert, which can be used for CSP installations. Currently, Egypt has one 140 MW solar thermal integrated combined-cycle power station with solar representing 20 MW of this capacity. Egypt targets to generate 8.1 GW from CSP plants in 2035. In this study, the CSP dynamic model is represented as in (24), which is given by [41].

$$\Delta P_{CSP} = \frac{K_{SCSP}}{T_{SCSP} s+1} * \frac{K_{TCSP}}{T_{TCSP} s+1} * \Delta P_{ST} \quad (24)$$

where K_{SCSP} and T_{SCSP} are solar collector gain and time constant, and K_{TCSP} and T_{TCSP} are thermal turbine gain and time constant. ΔP_{CSP} represents power change of CSP plants and ΔP_{ST} represents power change of solar thermal.

- **Wind power plants**

WG is one of the most promising RESs worldwide besides PV. Egypt has suitable locations for installing wind generation, particularly in the Gulf of Suez, a few locations beside the Nile river, locations in New Valley governorate, and locations in Sinai. Currently, Egypt produces 1375 MW from wind energy [42] and targets to generate 20.6 GW in 2035. In this study, the WG dynamic model is represented as in (25), which is given by [40].

$$\Delta P_{WG} = \left(\frac{K_{WG}}{T_{WG} s+1} \right) * \Delta P_{\mathrm{Wind}} \quad (25)$$

where K_{WG} and T_{WG} are wind generation gain and time constant. ΔP_{Wind} represents power change of wind and ΔP_{WG} represents power change of wind generation. Wind power plants power output is variable and difficult to predict because it depends on weather conditions (i.e., wind speed). Therefore, generally, it is treated as a non-dispatchable generation and represents a source of fluctuation and disturbance in the power system under study. Moreover, WG provides no inertia to the power system because it is usually connected to the grid through a power electronic-based converter. Consequently, it reduces the power system inertia. The low power system inertia makes the frequency deviations faster and larger.

C. DYNAMIC MODEL OF AGGREGATED ELECTRIC VECHICLES

Currently, most EVs are charged using an uncontrolled charging method. They are plugged in and charged at the maximum charging power until they are fully charged. This charging method is simple and fast, but it may cause many

This article has been accepted for publication in a future issue of this journal, but has not been fully edited. Content may change prior to final publication. Citation information: DOI 10.1109/ACCESS.2022.3174080, IEEE Access

negative impacts on the power system, and EVs cannot provide any grid services in this case [43], [44]. Another method of charging is smart charging, where EVs operate as controllable loads, and their charging power can be controlled depending on many parameters such as grid condition, electricity price, owner preferences, etc. [45], [46]. EVs can provide many grid services if a smart charging method is used. However, in this case, EV needs more time to charge than uncontrolled charging. A more advanced charging method is smart charging and discharging, where EVs charging and discharging are controlled. EVs' operation in discharging mode is referred to as vehicle-to-grid (V2G). In this method, EVs operate as energy storage, and they can provide many grid services even more than the smart charging method. However, in this case, bidirectional chargers are needed to allow the power to flow in two directions. It may harm EV battery lifetime due to continuous charging and discharging. Furthermore, EV needs more time for charging than uncontrolled and smart charging.

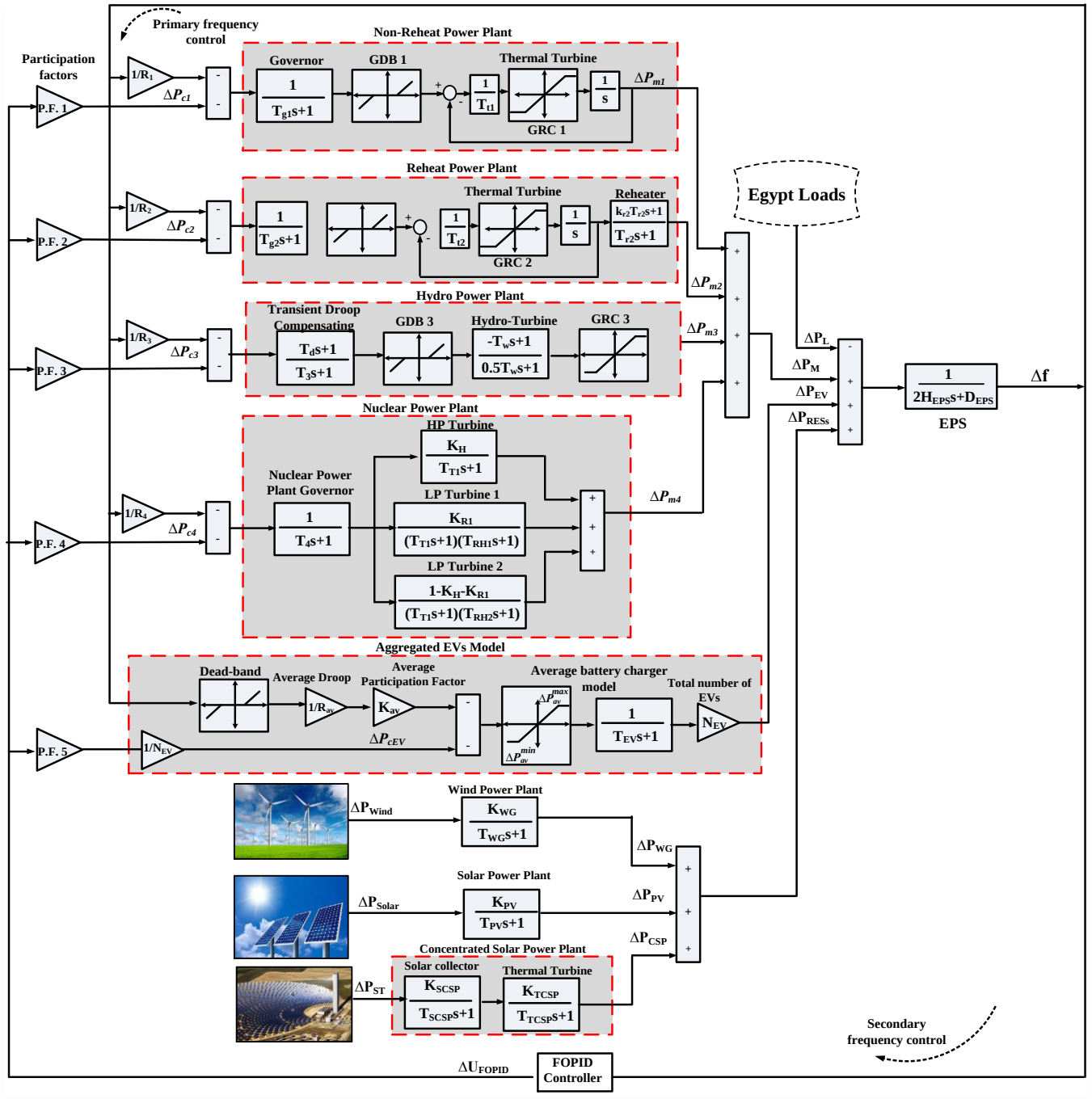

FIGURE 10. Block diagram of the EPS based on the future 2035 scenario.

This article has been accepted for publication in a future issue of this journal, but has not been fully edited. Content may change prior to final publication. Citation information: DOI 10.1109/ACCESS.2022.3174080, IEEE Access

The Egyptian government has not announced targets for the number of EVs in 2035. However, the IRENA report expected that EVs number in Egypt may reach 700,000 EVs in 2030. Therefore, it is expected that the number of EVs in Egypt to be more than 1 million in 2035. However, it is difficult to accurately estimate the number of EV owners willing to participate in ancillary services because it depends on the number of EVs in Egypt in 2035 and power system operators' incentives for EV owners to participate in grid services. Therefore, in this study, the maximum capacity of EVs participating in frequency regulation was assumed to be 6.6 GW. This value is calculated considering 6.6 kW charger capacity and 1 million EVs (i.e., 6.6 kW*1000000 = 6.6 GW). Note that the same capacity can be achieved by assuming a lower number of EVs and a higher EV chargers power rating.

In this study, EVs change charging/discharging of active power to enhance frequency stability and reduce frequency deviations resulting from the mismatch between supply and demand. The mismatch results from the continuous variation of loads and intermittent RESs generation in EPS. EVs can change their charging and discharging power very quickly because of the fast response of power electronic-based chargers. Consequently, EVs can have an important role in enhancing the frequency stability of future power systems.

The dynamic model of aggregated EVs that is used in this study is shown in Fig. 10. The first block from the left represents the dead band which is used to prevent continuous charging and discharging of EVs for small fluctuations in frequency to prolong EV batteries lifetime. The dead band's upper and lower limits are ±10 mHz. R_{av} represents the average droop coefficient of aggregated EVs. K_{av} is the average participation factor, and its value depends on the average SoC of aggregated EVs and their operating modes (i.e., charging, idle, etc.). K_{av} ranges from 0 to 1. In this study, its value is assumed to be 1. The next block represents the limits of the reserve where ΔP_{av}^{max} is the average upward reserve and ΔP_{av}^{min} is the average downward reserve. The next block is the transfer function of the bidirectional EV battery charger. T_{EV} is the average time constant of EV chargers. N_{EV} is the total number of EVs participating in frequency regulation. ΔP_{cEV} is the control signal from the secondary controller (i.e., FOPID controller) to aggregated EVs. ΔP_{EV} is the change of EVs charging/discharging power. $\Delta P_{EVs} > 0$ when EVs are discharging, and $\Delta P_{EVs} < 0$ when EVs are charging. ΔP_{EVs} can be calculated using (26).

$$\Delta P_{\mathrm{EVs}} = \left(-\Delta f * \frac{1}{R_{av}} * K_{av} - \Delta P_{cEV}\right) * \frac{N_{EV}}{T_{EV}s + 1} \quad (26)$$

Considering the dynamic model of different components of EPS presented in this section, power system inertia and damping coefficient, and primary and secondary control loops, frequency deviation is calculated using (27). H is inertia constant, D is damping coefficient, and ΔP_L is change in load power. All the parameters of EPS are provided in appendix 2.

$$\Delta f = \frac{1}{2Hs + D}(\Delta P_{m1} + \Delta P_{m2} + \Delta P_{m3} + \Delta P_{m4} + \Delta P_{PV} + \Delta P_{CSP} + \Delta P_{WG} + \Delta P_{EV} - \Delta P_L) \quad (27)$$

IV. FOPID CONTROLLER AND PROBLEM FORMULATION

A. FOPID CONTROLLER

FOPID controller is a type of fractional order controllers based on fractional calculus [47], [48]. For FOPID, the order of integration and differentiation can be any real number. This means the power of integration and differentiation can be a non-integer (i.e. fractional-order). The FOPID controller is considered as an extension of the PID controller. The controller transfer function is presented in (28) and its block diagram representation in Fig. 11.

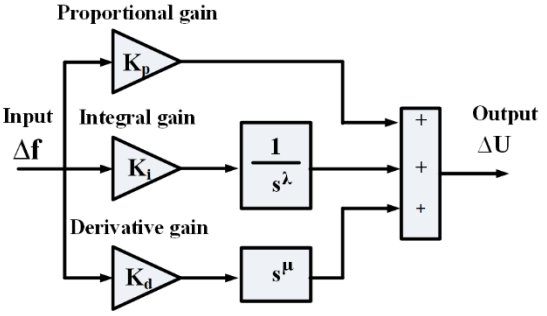

FIGURE 11. Structure of the FOPID controller.

$$G_{FOPID}(s) = K_p + \frac{K_i}{s^{\lambda}} + K_d s^{\mu} \quad (28)$$

where $G_{FOPID}(s)$ is the controller transfer function, K_p is the proportional gain, K_i is the integral gain, K_d is the derivative gain, and λ and μ are the fractional-order operators. λ and μ values are between 0 and 1. For the FOPID controller, the values of five parameters (i.e., K_p, K_i, K_d, λ, and μ) should be found accurately to achieve the required performance for different applications.

Many optimization algorithms were proposed in the literature to tune controller parameters in LFC studies. In this study RUN optimization algorithm is used to find the optimal parameters of the FOPID controller to achieve the best performance. The input to the FOPID controller is the error (i.e., frequency deviation in this study) and the output is the controller action (control signal to change the output power of conventional power plants and to change charging/discharging power of EVs). The effectiveness of the FOPID controller in improving the frequency stability of the EPS is tested by comparing its performance with PID,

This article has been accepted for publication in a future issue of this journal, but has not been fully edited. Content may change prior to final publication. Citation information: DOI 10.1109/ACCESS.2022.3174080, IEEE Access

PI, and I controllers. The RUN optimization algorithm is also used to tune PID, PI, and I controllers.

B. PROBLEM FORMULATION

Previous studies used many performance indices as objective functions to tune controller parameters. In this study, the ISE is selected as an objective function for the proper design of the proposed FOPID controller. The mathematical equation of ISE is presented in (29). The function of the proposed RUN optimizer is to minimize the ISE by finding optimal parameters of FOPID controller while considering optimization problem constraints. The constraints are the five parameters of the FOPID controller. The equations of the inequality constraints are presented in (30) to (34).

$$ISE = \int_0^{tsim} (\Delta f)^2 \, dt \tag{29}$$

$$K_p^{min} \le K_p \le K_p^{\max} \tag{30}$$

$$K_i^{min} \le K_i \le K_i^{\max} \tag{31}$$

$$K_d^{min} \le K_d \le K_d^{\max} \tag{32}$$

$$\lambda^{min} \le \lambda \le \lambda^{max} \tag{33}$$

$$\mu^{min} \le \mu \le \mu^{max} \tag{34}$$

where Δf is frequency deviation, t_{sim} and is the simulation time. K_p^{min}, K_i^{min}, and K_d^{min} are the minimum limits of the FOPID controller gains and K_p^{max}, K_i^{max}, and K_d^{max} are the maximum limits of the FOPID controller gains. Moreover, λ^{min} and μ^{min} are the minimum limits of fractional-order operators, and λ^{max} and μ^{max} are the maximum limits of fractional-order operators. The limits of K_p, K_i, and K_d, are 0 and 100 and limits of λ and μ are 0 and 1. The limits of I, PI, and PID controllers parameters are 0 and 100. The optimal parameters of the four controllers and the corresponding values of the objective function are given in Table 6.

V. RESULTS AND DISCUSSIONS

In this study, MATLAB/Simulink was used to model the dynamic model of the EPS considering RESs and perform simulations. Different scenarios are studied in the following subsections considering various disturbances and power system operating conditions.

A. SCENARIO 1: STEP LOAD INCREASE

In this section, the dynamic performance of the proposed FOPID controller is compared with PID and PI controllers under +0.2 pu SLP at time t = 20s. Fig. 12 (a) shows the dynamic performance of the three controllers without EVs participating in frequency regulation. Fig. 12 (b) shows the dynamic performance of the three controllers with EVs participating in frequency regulation. The results show that the proposed FOPID controller gives superior performance compared to PID and PI controllers for both cases. The FOPID controller results in the best performance with less overshoot, less undershoot, and faster settling time. While the PID controller showed a good performance and the PI controller provided the worst performance compared to other controllers. However, the EPS showed high-frequency stability for all studied controllers.

Considering that the FOPID controller resulted in the best dynamic response compared to other controllers, the effectiveness of EVs participation in frequency regulation will be studied while using the FOPID controller for LFC. Fig. 12 (c) shows the dynamic performance of the FOPID controller with and without EVs participating in frequency regulation to test the significance of EVs participation in frequency control. The results prove that EVs' participation in frequency regulation improved the dynamic response of the EPS and showed less overshoot and less undershoot. Considering the popularity of using the integral (I) controller in LFC in practice, the performance of the I controller is tested in the EPS for the future 2035 scenario and with a 0.2 pu SLP at time t =20s. The optimal value of K_i is found using the RUN algorithm, and it is given in Table 6. The results showed that the I controller could not suppress disturbances in the EPS and resulted in continuous frequency oscillations for both cases with/without EVs as demonstrated in Fig. 12 (d). Due to the poor performance of the I controller, the proposed FOPID controller is compared with PID and PI controllers only in the following scenarios.

B. SCENARIO 2: RANDOM STEP CHANGE OF LOAD

In this scenario, the frequency stability will be tested considering various step load changes (increase and decrease of load). Fig. 13 Shows the studied load variations during the simulation time. Fig. 14 (a) shows the dynamic performance of the three controllers without EVs participating in frequency regulation. Fig. 14 (b) shows the dynamic performance of the three controllers with EVs participating in frequency regulation. The results show that the proposed FOPID controller outperforms the other controllers for both cases. Fig. 14 (c) shows the dynamic performance of the FOPID controller with and without EVs participating in frequency regulation to test the significance of EVs participation in frequency control. The results prove that EVs participation in frequency regulation improved the dynamic response of the EPS subjected to different large disturbances.

C. SCENARIO 3: LARGE CHANGE IN RESs GENERATION

The high penetration of the intermittent and unpredictable RESs in the EPS could result in high fluctuations of the generated power. Therefore, in this scenario, large variations of intermittent RESs are studied. Fig. 15 shows the considered variations of RESs generated power. Fig. 16 shows the corresponding dynamic response for FOPID, PID, and PI controllers. Fig. 16 (a) shows the EPS performance without EVs' contribution, Fig. 16 (b) shows the EPS performance with EVs' contribution, and Fig. 16 (c)

This article has been accepted for publication in a future issue of this journal, but has not been fully edited. Content may change prior to final publication. Citation information: DOI 10.1109/ACCESS.2022.3174080, IEEE Access

shows the performance of the FOPID controller for the frequency stability of the EPS with/without EVs. The results showed that the proposed optimal FOPID controller based on the RUN optimization algorithm can provide better performance than PID and PI controllers when there are high fluctuations of RESs generation for all the studies cases. Moreover, EVs participation in frequency regulation of the EPS can reduce the frequency deviation caused by the large change in the generation of RESs.

Table 6. Optimal parameters of EPS controllers tuned using RUN algorithm

	Controller	ISE	K_p	K_i	K_d	λ	μ	N
Without EVS	FOPID	8.079E-05	100	99.9925	99.9425	0.5818	0.9998	-
	PID	9.770E-05	100	52.4492	63.6033	-	-	99.9933
	PI	3.035E-04	56.3393	14.8063	-	-	-	-
	I	6.941E-2	-	1.2196	-	-	-	-
With EVs	FOPID	3.832E-05	100	100	96.9305	0.7169	0.9081	-
	PID	4.508E-05	100	88.9035	61.3064	-	-	99.961
	PI	1.261E-04	100	25.3081	-	-	-	-
	I	9.680E-3	-	5.3539	-	-	-	-

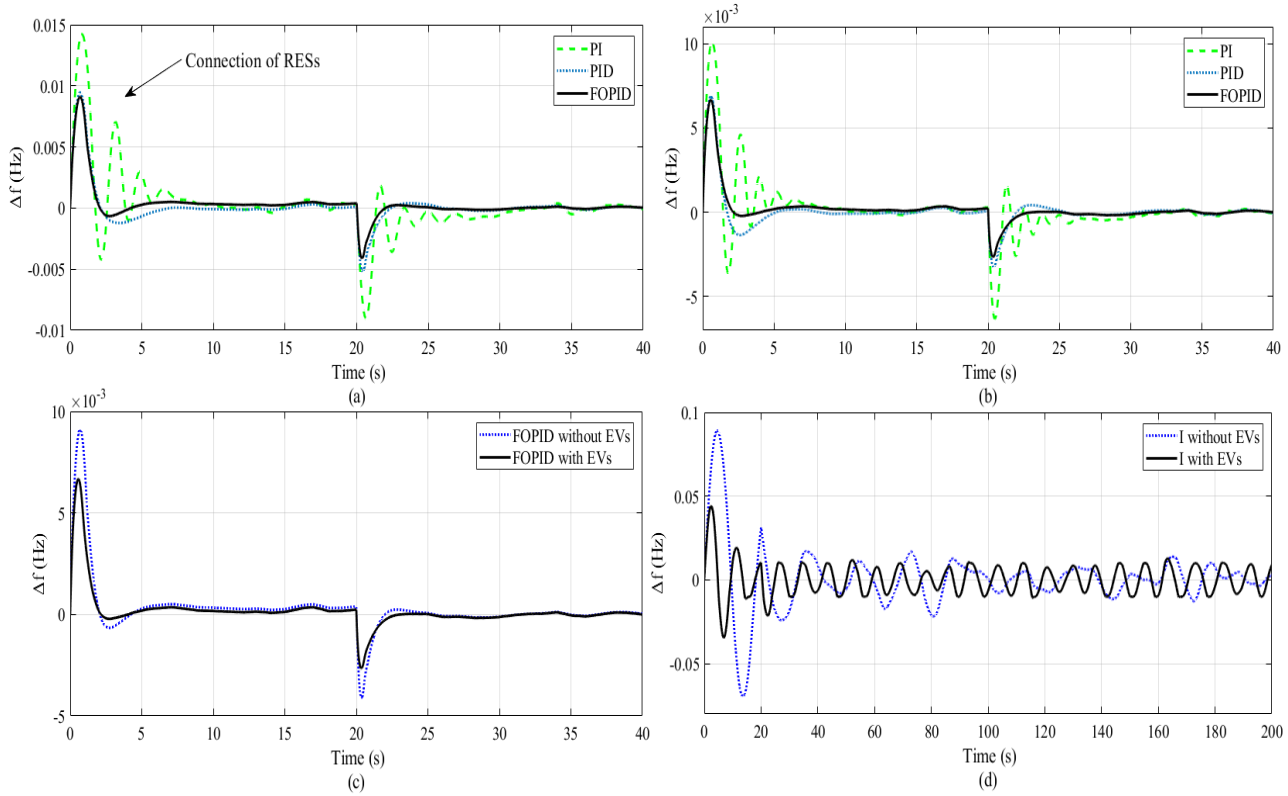

FIGURE 12. Scenario 1: Frequency deviation for step change of load. (a) EPS without EVs, (b) EPS with EVs, (c) the proposed FOPID controller with/without EVs, and (d) I controller with/without EVs.

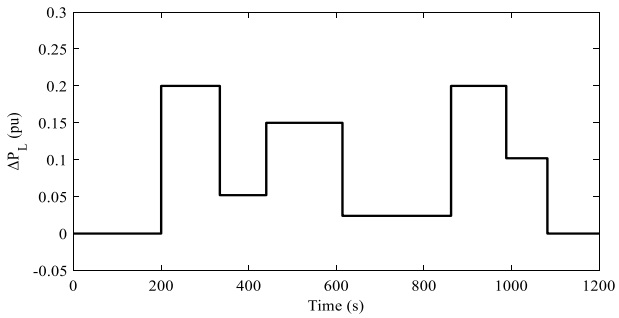

FIGURE 13. Random step change of load.

D. ROBUSTNESS TO PARAMETERS CHANGE

To test the robustness of the proposed FOPID controller based on the RUN optimization algorithm, the nominal value of the EPS inertia constant (*H*) is changed. The parameter value is changed by ±25% and ±50% without re-tuning the proposed FOPID controller and other controllers used in the previous scenarios. Fig. 17 shows the dynamic response of the EPS with +25% and +50% change in *H* considering 0.2 pu SLP at time t = 20s for both cases with/without EVs. All the controllers showed a good performance, and the proposed FOPID controller achieved the best performance. Fig. 18 shows the dynamic response of the EPS with -25% and -50% change in *H*. The proposed

This article has been accepted for publication in a future issue of this journal, but has not been fully edited. Content may change prior to final publication. Citation information: DOI 10.1109/ACCESS.2022.3174080, IEEE Access

FOPID controller showed a better performance compared to the PID controller as shown in Fig. 18 (a)-(d). The good dynamic responses achieved prove the robustness of the proposed FOPID controller to variations in EPS conditions and the unnecessity to optimize controller parameters again for continuous variations in power system conditions. In addition, RUN-PID showed a robust performance with changes of *H*. However, the PI controller was unable to suppress frequency fluctuations in the EPS and resulted in instability when the H value changed by -50% for the case without EVs as shown in Fig. 18(c). The participation of EVs in frequency control enabled the PI controller to suppress the frequency fluctuations and prevented the EPS of reaching frequency instability as shown in Fig. 18(d).

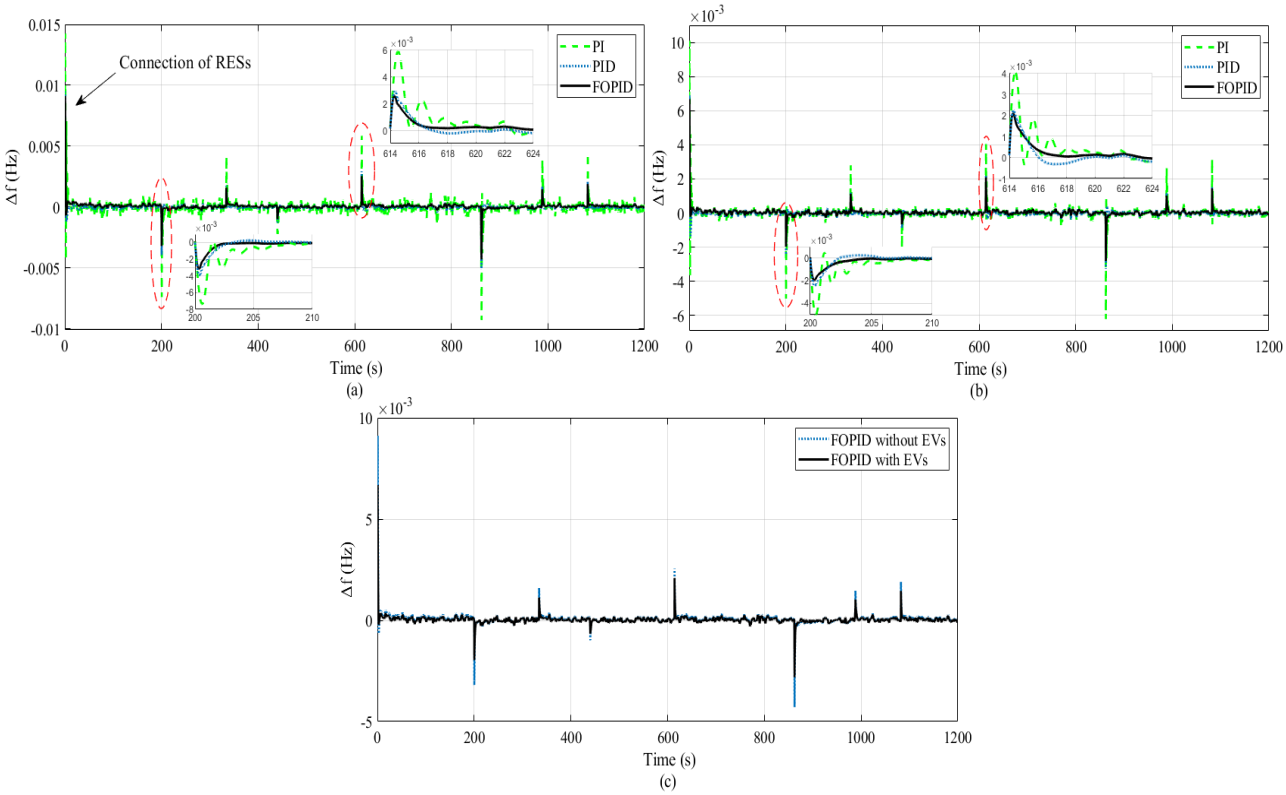

FIGURE 14. Scenario 2: Frequency deviation with random step change of load. (a) EPS without EVs, (b) EPS with EVs, and (c) FOPID controller with/without EVs.

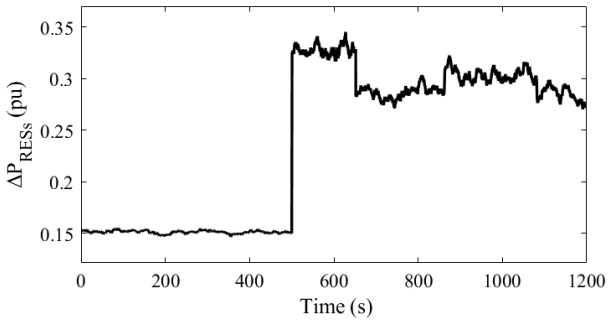

FIGURE 15. RESs power variation for scenario 3.

VII. CONCLUSION

In this study, the frequency stability of Egyptian Power System (EPS) in the 2035 future scenario was assessed. The results showed that EPS in the 2035 future scenario has high-frequency stability even with the increased penetration of renewable energy sources. Additionally, the FOPID controller optimized by RUNge Kutta optimizer (RUN) gives a better performance than PID, PI, and I controllers at different operation scenarios and different power system disturbances. Moreover, the results proved that electric vehicles (EVs) could enhance the frequency stability of the EPS when they participate in frequency regulation service and could prevent power system instability for low inertia power systems. Furthermore, the RUN algorithm proved its effectiveness over other optimization algorithms (i.e., particle swarm optimization and artificial bee colony) for the load frequency control applications. In future work we will test the performance of other controllers in EPS at 2035 future scenario. Moreover, we will try to improve the RUN algorithm to provide a better performance at LFC application.

It is essential to mention that there are no regulations in Egypt organizing the participation of distributed energy resources in general and EVs specifically in providing grid-wide services such as frequency regulation or local services such as voltage regulation, congestion management, etc. Therefore, Egyptian regulatory authorities must prepare regulations that allow EVs' participation in frequency

This article has been accepted for publication in a future issue of this journal, but has not been fully edited. Content may change prior to final publication. Citation information: DOI 10.1109/ACCESS.2022.3174080, IEEE Access

regulations and clarify the requirements of EVs for participation and the economic incentives to EVs owners to participate in frequency regulation. Moreover, infrastructure investment at the distribution system is required to enable frequency regulation service from EVs, such as communication infrastructure, bidirectional EV chargers, etc. Therefore, a cost-benefit analysis of EVs' participation in frequency regulation in EPS is essential to assess its economic feasibility from a system-wide perspective.

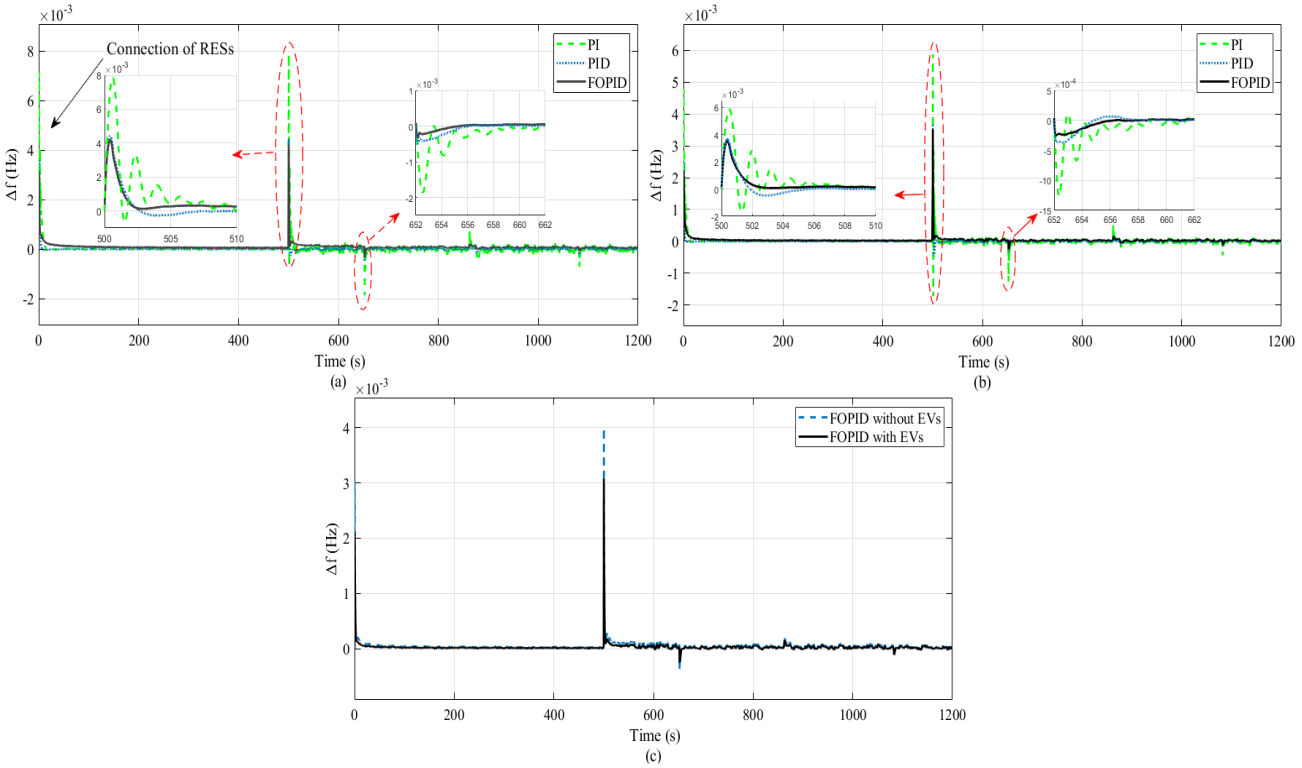

FIGURE 16. Scenario 3: Frequency deviation with large variation in RESs generation. (a) EPS without EVs, (b) EPS with EVs, and (c) FOPID without and with EVs.

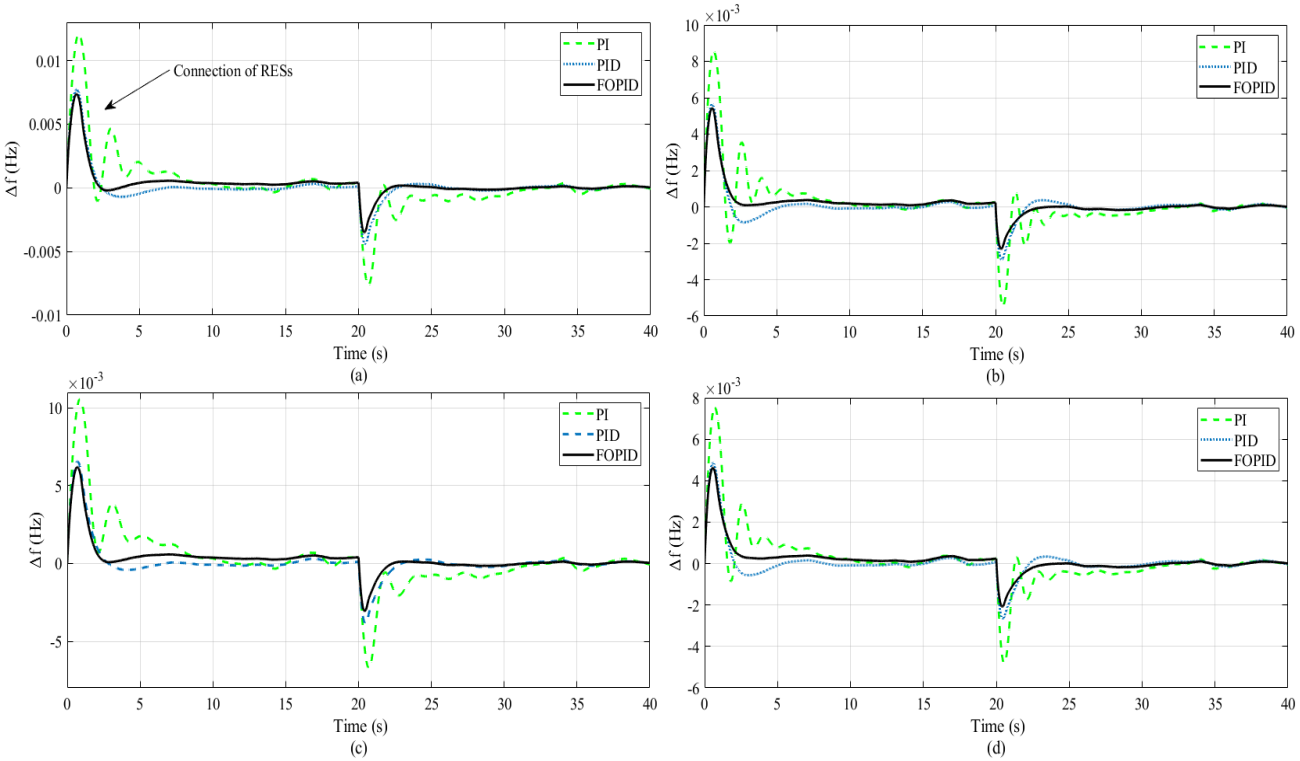

FIGURE 17. Scenario 4: Frequency deviation with change in system inertia H. (a) EPS without EVs if H changes by +25%, (b) EPS with EVs if H changes by +25%, (c) EPS without EVs if H changes by +50%, (d) EPS with EVs if H changes by +50%.

This article has been accepted for publication in a future issue of this journal, but has not been fully edited. Content may change prior to final publication. Citation information: DOI 10.1109/ACCESS.2022.3174080, IEEE Access

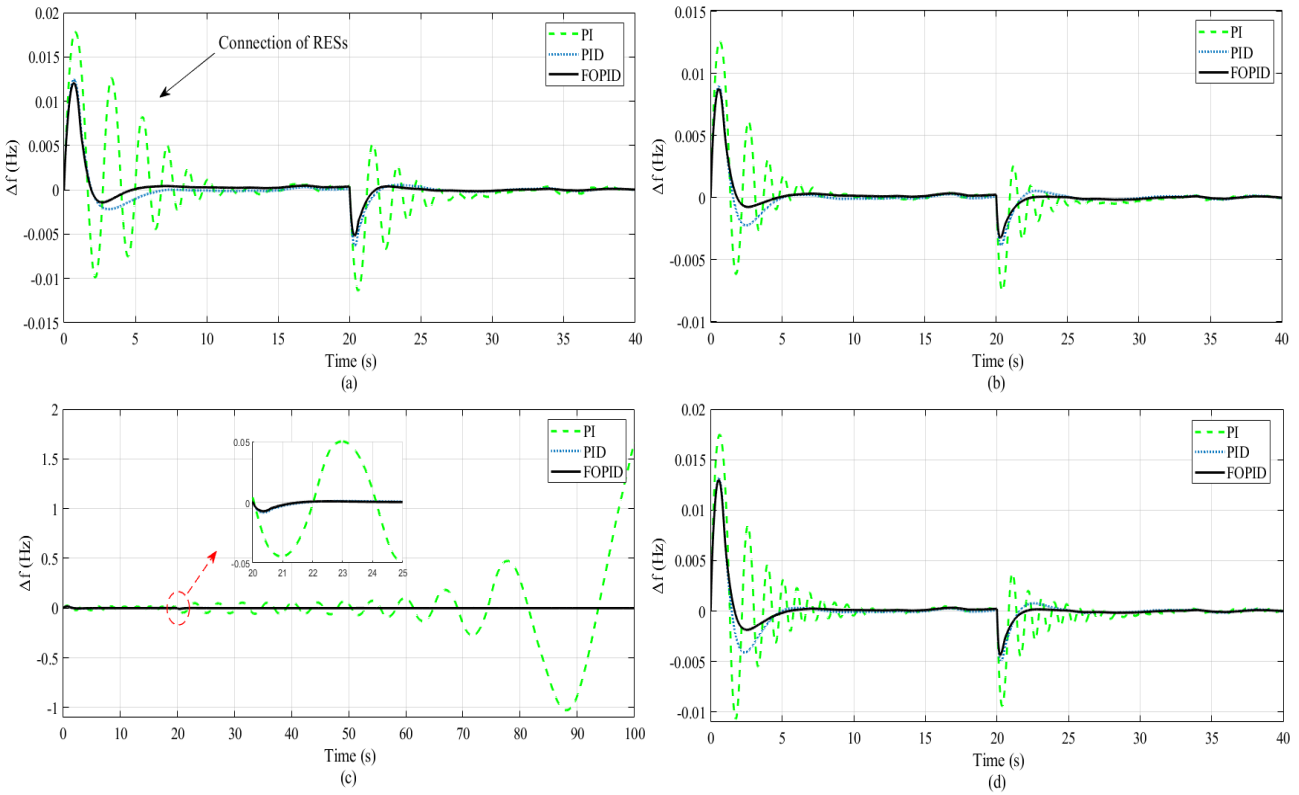

FIGURE 18. Scenario 4: Frequency deviation with change in system inertia H. (a) EPS without EVs if H changes by -25%, (b) EPS with EVs if H changes by -25%, (c) EPS without EVs if H changes by -50%, (d) EPS with EVs if H changes by -50%.

APPENDICES

APPENDIX 1

Parameters of two area power system [35].

K_{ps} = 120 Hz/pu MW, T_{ps} = 20 s, T_g = 0.08 s, T_t = 0.3 s, k_r = 0.5, T_r = 10 s, R = 2.4 Hz/pu MW, B = 0.425 pu MW/Hz, and T_{tie} = 0.086.

APPENDIX 2

Parameters of the Egyptian power system (EPS).

H = 4.07 s, D = 0.028 pu MW/Hz, T_{g1} = *0.08 s*, T_{t1} = *0.3 s*, T_{g2} = *0.08 s*, T_{t2} = *0.3 s*, , k_{r2} = 0.5, T_{r2} = 10 s, T_3 = 90 s, T_d = 5 s, T_w = 1 s, R_1 = 2.5 Hz/pu MW, R_2 = 2.5 Hz/pu MW, R_3 = 1 Hz/pu MW, f = 50 Hz, K_{PV} = 1, T_{PV} = 1.85 s, K_{WG} = 1, T_{WG} = 1.5 s, K_{SCSP} = 1.8, T_{SCSP} = 1.8 s, K_{TCSP} = 1, T_{TCSP} = 0.3 s, T_4 = 0.08 s, K_H = 2, T_{T1} = 0.5 s, K_{R1} = 0.3, T_{RH1} = 7 s, T_{RH2} = 9 s. For the case without EVs *P.F.1* = 0.45, *P.F.2* = 0.45, *P.F.3* = 0.04, and *P.F.4* = 0.06. For the case with EVs *P.F.1* = 0.42, *P.F.2* = 0.42, *P.F.3* = 0.03, *P.F.4* = 0.05, and *P.F.5* = 0.08.

REFERENCES

[1] M. M. Gamil *et al.*, "Optimal sizing of a residential microgrid in Egypt under deterministic and stochastic conditions with PV/WG/Biomass Energy integration," *AIMS Energy 2021 3483*, vol. 9, no. 3, pp. 483–515, 2021.

[2] A. K. Barik and D. C. Das, "Integrated resource planning in sustainable energy-based distributed microgrids," *Sustain. Energy Technol. Assessments*, vol. 48, p. 101622, Dec. 2021.

[3] International Renewable Energy Agency (IRENA), *Global Renewables Outlook: Energy transformation 2050*. 2020.

[4] R. Yan, N. Al-Masood, T. Kumar Saha, F. Bai, and H. Gu, "The anatomy of the 2016 South Australia blackout: A catastrophic event in a high renewable network," *IEEE Trans. Power Syst.*, vol. 33, no. 5, pp. 5374–5388, Sep. 2018.

[5] M. Dreidy, H. Mokhlis, and S. Mekhilef, "Inertia response and frequency control techniques for renewable energy sources: A review," *Renew. Sustain. Energy Rev.*, vol. 69, no. July 2016, pp. 144–155, 2017.

[6] Y. Ye, Y. Qiao, and Z. Lu, "Revolution of frequency regulation in the converter-dominated power system," *Renew. Sustain. Energy Rev.*, vol. 111, no. May 2018, pp. 145–156, 2019.

[7] Y. Arya *et al.*, "Cascade-IλDμN controller design for AGC of thermal and hydro-thermal power systems integrated with renewable energy sources," *IET Renew. Power Gener.*, vol. 15, no. 3, pp. 504–520, Feb. 2021.

[8] R. Shankar, K. Chatterjee, and R. Bhushan, "Impact of energy storage system on load frequency control for diverse sources of interconnected power system in deregulated power environment," *Int. J. Electr. Power Energy Syst.*, vol. 79, pp. 11–26, 2016.

[9] M. E. Lotfy, T. Senjyu, M. A. F. Farahat, A. F. Abdel-Gawad, and A. Yona, "A frequency control approach for hybrid power system using multi-objective optimization," *Energies*, vol. 10, no. 1, pp. 1–22, 2017.

[10] Y. Arya, N. Kumar, and S. K. Gupta, "Optimal automatic generation control of two-area power systems with energy storage units under deregulated environment," *J. Renew. Sustain. Energy*, vol. 9, no. 6, p. 064105, Dec. 2017.

[11] D. Khamari, R. K. Sahu, and S. Panda, "A Modified Moth Swarm Algorithm-Based Hybrid Fuzzy PD–PI Controller for Frequency Regulation of Distributed Power Generation System with Electric Vehicle," *J. Control. Autom. Electr. Syst.*, vol. 31, no. 3, pp. 675–692, 2020.

[12] G. Magdy, M. Nour, G. Shabib, A. A. Elbaset, and Y. Mitani, "Supplementary Frequency Control in a High-penetration Real Power System by Renewables Using SMES Application Electrical Electrical Electrical Electrical Systems Systems Systems Systems," *J. Electr. Syst.*, vol. 15, no. 4, pp. 526–538, 2019.

[13] Y. Xu, C. Li, Z. Wang, N. Zhang, and B. Peng, "Load Frequency Control of a Novel Renewable Energy Integrated Micro-Grid Containing Pumped Hydropower Energy Storage," *IEEE Access*, vol. 6, pp. 29067–29077, 2018.

[14] J. Kim *et al.*, "Supercapacitor to Provide Ancillary Services with Control Coordination," *IEEE Trans. Ind. Appl.*, vol. 55, no. 5, pp. 5119–5127, 2019.

[15] A. Pappachen and A. Peer Fathima, "Critical research areas on load frequency control issues in a deregulated power system: A state-of-the-art-of-review," *Renew. Sustain. Energy Rev.*, vol. 72, no. January, pp. 163–177, 2017.

[16] I. E. A. (IEA), "Global EV Outlook 2020 – Analysis - IEA," 2020. [Online]. Available: https://www.iea.org/reports/global-ev-outlook-2020. [Accessed: 28-Feb-2021].

[17] G. Magdy, A. Bakeer, and M. Alhasheem, "Robust decentralized model predictive load-frequency control design for time-delay renewable power systems," *Int. J. Emerg. Electr. Power Syst.*, vol. 22, no. 5, pp. 617–628, Oct. 2021.

[18] V. Skiparev, J. Belikov, and E. Petlenkov, "Reinforcement learning based approach for virtual inertia control in microgrids with renewable energy sources," *IEEE PES Innov. Smart Grid Technol. Conf. Eur.*, vol. 2020-October, pp. 1020–1024, Oct. 2020.

[19] F. Yang, X. Shao, S. M. Muyeen, D. Li, S. Lin, and C. Fang, "Disturbance Observer Based Fractional-Order Integral Sliding Mode Frequency Control Strategy for Interconnected Power System," *IEEE Trans. Power Syst.*, vol. 36, no. 6, pp. 5922–5932, Nov. 2021.

[20] H. A. Yousef, K. AL-Kharusi, M. H. Albadi, and N. Hosseinzadeh, "Load Frequency Control of a Multi-Area Power System: An Adaptive Fuzzy Logic Approach," *IEEE Trans. Power Syst.*, vol. 29, no. 4, pp. 1822–1830, Jul. 2014.

[21] M. Sharma, S. Dhundhara, Y. Arya, and S. Prakash, "Frequency stabilization in deregulated energy system using coordinated operation of fuzzy controller and redox flow battery," *Int. J. Energy Res.*, vol. 45, no. 5, pp. 7457–7475, Apr. 2021.

[22] G. Sharma, A. Panwar, Y. Arya, and M. Kumawat, "Integrating layered recurrent ANN with robust control strategy for diverse operating conditions of AGC of the power system," *IET Gener. Transm. Distrib.*, vol. 14, no. 18, pp. 3886–3895, Sep. 2020.

[23] G. Magdy, H. Ali, and D. Xu, "Effective control of smart hybrid power systems: Cooperation of robust LFC and virtual inertia control system," *CSEE J. Power Energy Syst.*, 2021.

[24] H. M. Hasanien, "Whale optimisation algorithm for automatic generation control of interconnected modern power systems including renewable energy sources," *IET Gener. Transm. Distrib.*, vol. 12, no. 3, pp. 607–614, Feb. 2018.

[25] M. Sharma, S. Dhundhara, Y. Arya, and S. Prakash, "Frequency excursion mitigation strategy using a novel COA optimised fuzzy controller in wind integrated power systems," *IET Renew. Power Gener.*, vol. 14, no. 19, pp. 4071–4085, Dec. 2020.

[26] Y. Arya, P. Dahiya, E. Çelik, G. Sharma, H. Gözde, and I. Nasiruddin, "AGC performance amelioration in multi-area interconnected thermal and thermal-hydro-gas power systems using a novel controller," *Eng. Sci. Technol. an Int. J.*, vol. 24, no. 2, pp. 384–396, Apr. 2021.

[27] P. Dahiya, P. Mukhija, A. R. Saxena, and Y. Arya, "Comparative performance investigation of optimal controller for AGC of electric power generating systems," *https://doi.org/10.7305/automatika.2017.12.1707*, vol. 57, no. 4, pp. 902–921, 2018.

[28] M. Nour, J. P. Chaves-Ávila, G. Magdy, and Á. Sánchez-Miralles, "Review of positive and negative impacts of electric vehicles charging on electric power systems," *Energies*, vol. 13, no. 18, pp. 1–32, 2020.

[29] C. Peng, J. Zou, and L. Lian, "Dispatching strategies of electric vehicles participating in frequency regulation on power grid: A review," *Renew. Sustain. Energy Rev.*, vol. 68, no. July 2016, pp. 147–152, 2017.

[30] J. Zhong *et al.*, "Coordinated control for large-scale EV charging facilities and energy storage devices participating in frequency regulation," *Appl. Energy*, vol. 123, pp. 253–262, 2014.

[31] S. Debbarma and A. Dutta, "Utilizing electric vehicles for LFC in restructured power systems using fractional order controller," *IEEE Trans. Smart Grid*, vol. 8, no. 6, pp. 2554–2564, 2017.

[32] H. Abubakr, T. H. Mohamed, M. M. Hussein, J. M. Guerrero, and G. Agundis-Tinajero, "Adaptive frequency regulation strategy in multi-area microgrids including renewable energy and electric vehicles supported by virtual inertia," *Int. J. Electr. Power Energy Syst.*, vol. 129, no. August 2020, p. 106814, 2021.

[33] S. Ranjan, D. C. Das, A. Latif, and N. Sinha, "Electric vehicles to renewable-three unequal areas-hybrid microgrid to contain system frequency using mine blast algorithm based control strategy," *Int. J. Syst. Assur. Eng. Manag.*, vol. 12, no. 5, pp. 961–975, 2021.

[34] International Renewable Energy Agency (IRENA), *Renewable Energy Outlook: Egypt*. 2018.

[35] H. Gozde, M. Cengiz Taplamacioglu, and I. Kocaarslan, "Comparative performance analysis of Artificial Bee Colony algorithm in automatic generation control for interconnected reheat thermal power system," *Int. J. Electr. Power Energy Syst.*, vol. 42, no. 1, pp. 167–178, 2012.

[36] I. Ahmadianfar, A. A. Heidari, A. H. Gandomi, X. Chu, and H. Chen, "RUN beyond the metaphor: An efficient optimization algorithm based on Runge Kutta method," *Expert Syst. Appl.*, vol. 181, p. 115079, Nov. 2021.

[37] Y. L. Abdel-Magid and M. A. Abido, "AGC tuning of interconnected reheat thermal systems with particle swarm optimization," *Proc. IEEE Int. Conf. Electron. Circuits, Syst.*, vol. 1, pp. 376–379, 2003.

[38] G. Magdy, A. Bakeer, M. Nour, and E. Petlenkov, "A New Virtual Synchronous Generator Design Based on the SMES System for Frequency Stability of Low-Inertia Power Grids," *Energies 2020, Vol. 13, Page 5641*, vol. 13, no. 21, p. 5641, Oct. 2020.

[39] B. Mohanty, "TLBO optimized sliding mode controller for multi-area multi-source nonlinear interconnected AGC system," *Int. J. Electr. Power Energy Syst.*, vol. 73, pp. 872–881, 2015.

[40] G. Magdy, G. Shabib, A. A. Elbaset, and Y. Mitani, "Renewable power systems dynamic security using a new coordination of frequency control strategy based on virtual synchronous generator and digital frequency protection," *Int. J. Electr. Power Energy Syst.*, vol. 109, pp. 351–368, Jul. 2019.

[41] D. C. Das, A. K. Roy, and N. Sinha, "GA based frequency controller for solar thermal-diesel-wind hybrid energy generation/energy storage system," *Int. J. Electr. Power Energy Syst.*, vol. 43, no. 1, pp. 262–279, 2012.

[42] New and Renewable Energy Authority (NREA), "Egypt wind power capacity 2021," Jan-2021. [Online]. Available: http://nrea.gov.eg/Content/reports/jan2021En.jpg. [Accessed: 27-Feb-2021].

[43] M. Nour, A. Ali, and C. Farkas, "Mitigation of Electric Vehicles Charging Impacts on Distribution Network with Photovoltaic Generation," *Proc. 2019 Int. Conf. Innov. Trends Comput. Eng. ITCE 2019*, pp. 384–388, 2019.

[44] M. Nour, H. Ramadan, A. Ali, and C. Farkas, "Impacts of plug-in electric vehicles charging on low voltage distribution network," in *Aswan International Workshop on Computational Methods in Power Systems (CMPS 2018)*, 2018.

[45] M. Nour, S. M. Said, H. Ramadan, A. Ali, and C. Farkas, "Control of Electric Vehicles Charging Without Communication Infrastructure," *2018 20th Int. Middle East Power Syst. Conf. MEPCON 2018 - Proc.*, pp. 773–778, 2019.

[46] H. Ramadan, A. Ali, M. Nour, and C. Farkas, "Smart Charging and Discharging of Plug-in Electric Vehicles for Peak Shaving and Valley Filling of the Grid Power," *2018 20th Int. Middle East Power Syst. Conf. MEPCON 2018 - Proc.*, pp. 735–739, 2019.

[47] D. Xue and Y. Q. Chen, "A comparative introduction of four fractional order controllers," in *Proceedings of the World Congress on Intelligent Control and Automation (WCICA)*, 2002, vol. 4, pp. 3228–3235.

[48] A. Tepljakov *et al.*, "Towards Industrialization of FOPID Controllers: A Survey on Milestones of Fractional-Order Control and Pathways for Future Developments," *IEEE Access*, vol. 9, pp. 21016–21042, 2021.

This article has been accepted for publication in a future issue of this journal, but has not been fully edited. Content may change prior to final publication. Citation information: DOI 10.1109/ACCESS.2022.3174080, IEEE Access

Morsy Nour received the bachelor's degree in electrical power engineering from Aswan University, Aswan, Egypt, and the M.Sc. degree in electrical engineering from Budapest University of Technology and Economics, Budapest, Hungary. He is currently pursuing the Ph.D. degree in electrical engineering at Comillas Pontifical University, Madrid, Spain. Since 2013 he has been working as a Teaching Assistant at Faculty of Energy Engineering, Aswan University, Aswan, Egypt and currently, he is a Research Assistant at the Institute for Research in Technology (IIT), Comillas Pontifical University, Madrid, Spain. His research interest includes integration of electric vehicles into electric power systems, load frequency control, blockchain applications in electricity sector, and peer to peer energy trading.

Gaber Magdy is a faculty member at Aswan University, Aswan, Egypt. He received the B.Sc. and M.Sc. (Hons.) degrees in Electrical Engineering from Aswan University, Egypt, in 2011 and 2014, respectively. In 2019, he received a jointly-supervised PhD degree in Electrical Engineering from Minia University, Egypt (Main university), and Kyushu Institute of Technology, Japan (Host university). Since December 2011, he joined the Electrical Engineering Department, Faculty of Energy Engineering, Aswan University, Aswan, Egypt, first as a Demonstrator and then as an Assistant Lecturer in November 2014. From 2017 to 2019, he was a researcher in the Department of Electrical and Electronic Engineering, Kyushu Institute of Technology, Japan. He is currently an assistant professor at the Department of Electrical Engineering, Faculty of Energy Engineering, Aswan University, Aswan, Egypt. He has authored /co-authored two international books and over 50 peer-reviewed papers on renewable power systems stability, dynamics, and control. His research interests include power system stability, smart/micro-grid dynamics and control, renewable energies, energy storage systems, and digital control techniques, all of which are applied to electric power systems.

José Pablo Chaves-Ávila obtained the Bachelor in Economics in University of Costa Rica (Costa Rica) in 2008. As part of the Erasmus Mundus master in Economics and Management of Network Industries, he holds the Master in the Electric Power Industry from Engineering School (ICAI) of the Comillas Pontifical University and the master in Digital Economics and Network Industries from Paris Sud-11 University (Paris, France). In 2014 he obtained the Erasmus Mundus Joint Doctorate on Sustainable Energy Technologies and Strategies Degree at Delft University of Technology (The Netherlands), a joint program with Comillas Pontifical University and the Royal Institute of Technology (KTH), Sweden. He is a researcher at the Institute for Research in Technology (IIT) at the Engineering School (ICAI) of the Comillas Pontifical University. He has been visiting scholar at the European University Institute (Italy), the Lawrence Berkeley National Laboratory (USA) and the Massachusetts Institute of Technology (MIT), USA. From September 2016 he is lead and operating agent of the ISGAN Academy of the International Smart Grid Action Network. In August 2020 he was selected as a member of the Expert list of the Regional Commission of the Electrical Interconnection for Central American (CRIE) and in September 2021 was appointed as a member of the ACER Expert Group on Demand Side Flexibility for EU Agency for the Cooperation of Energy Regulators (ACER). His areas of interest are Energy Economics, integration of renewable resources and distributed energy resources in the electricity sector, smart grids and regulation of the electricity and other energy sectors.

Álvaro Sánchez-Miralles holds a Doctor's degree in Engineering Sciences from Comillas Pontifical University. He is an Associate Professor at the Electronics and Automation Engineering Department. He has participated in more than 60 consultancy and research projects for several Spanish and foreign firms and regulatory commissions, related with the energy industry. He has published more than 50 scientific publications. In 2012, he received the "2012 IBM Enterprising Award.
His main fields of interest are smart grids and smart cities: integration of renewable generation and storage in distribution networks (smart storage, microgrids), electric vehicles (V2G and VPP), planning power grids (reference network models, system planning with central and distributed energy resources evolution and tariff design) and energy management in buildings and districts (aggregation of prosumers with market price maker and taker participation, microgrids, building and home energy management systems, electric and thermal synergies optimization).

Eduard Petlenkov received the B.Sc., M.Sc., and Ph.D. degrees in computer and systems engineering from the Tallinn University of Technology. He is currently a Professor with the Department of Computer Systems, Tallinn University of Technology. His main research interests include the domain of nonlinear control, system analysis, and computational intelligence.